Journal Pre-proofs

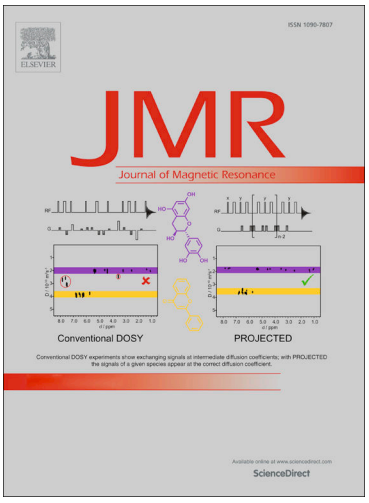


# Reducing the Effects of Weak Homonuclear Dipolar Coupling with CPMG Pulse Sequences for Static and Spinning Solids

Adam R. Altenhof, Zhehong Gan, Robert W. Schurko

PII: S1090-7807(22)00032-5
DOI: https://doi.org/10.1016/j.jmr.2022.107174
Reference: YJMRE 107174

To appear in: *Journal of Magnetic Resonance*

Received Date: 10 January 2022
Revised Date: 18 February 2022
Accepted Date: 21 February 2022

Please cite this article as: A.R. Altenhof, Z. Gan, R.W. Schurko, Reducing the Effects of Weak Homonuclear Dipolar Coupling with CPMG Pulse Sequences for Static and Spinning Solids, *Journal of Magnetic Resonance* (2022), doi: https://doi.org/10.1016/j.jmr.2022.107174

This is a PDF file of an article that has undergone enhancements after acceptance, such as the addition of a cover page and metadata, and formatting for readability, but it is not yet the definitive version of record. This version will undergo additional copyediting, typesetting and review before it is published in its final form, but we are providing this version to give early visibility of the article. Please note that, during the production process, errors may be discovered which could affect the content, and all legal disclaimers that apply to the journal pertain.

© 2022 Published by Elsevier Inc.

Journal Pre-proofs

# Reducing the Effects of Weak Homonuclear Dipolar Coupling with CPMG Pulse Sequences for Static and Spinning Solids

Adam R. Altenhof[1,2], Zhehong Gan[2], and Robert W. Schurko[1,2,*]

1. Department of Chemistry and Biochemistry, Florida State University, Tallahassee, FL 32306, USA

2. National High Magnetic Field Laboratory, 1800 East Paul Dirac Drive, Tallahassee, FL 32310, USA

*Author to whom correspondence should be addressed.

E-mail: rschurko@fsu.edu

Tel: (850)-645-8614

Journal Pre-proofs

**Abstract**

The Carr-Purcell/Meiboom-Gill (CPMG) pulse sequence, initially introduced for measuring transverse relaxation time constants ($T_2$), can provide significant signal enhancements for solid-state NMR (SSNMR) spectra. The proper implementation of CPMG for acquiring spectra influenced by chemical shift anisotropies (CSAs), first and/or second order quadrupolar interactions, or paramagnetic broadening has been well documented to date, as have the effects

of heteronuclear dipolar coupling on CPMG echo trains and $T_2$ lifetimes. Homonuclear dipolar coupling can also impact $T_2$ lifetimes and CPMG echo trains; these effects have been thoroughly investigated for spectra of homonuclear dipolar coupled spin-1/2 nuclei typically acquired under static conditions that are predominantly influenced by dipolar broadening (*e.g.*, $^{1}$H, $^{19}$F, *etc*.). In particular, it has been shown that short refocusing pulses with small flip angles can extend the effective $T_2$ ($T_2^{\text{eff}}$, the observed $T_2$ constant as impacted by experimental conditions) measured by CPMG sequences for strong homonuclear dipolar coupled spin-1/2 pairs under static conditions. To date, these effects have not been explored for (i) spin-1/2 nuclei that have significant CSAs and simultaneously feature weak homonuclear dipolar couplings, (ii) for quadrupolar nuclei that are also weakly homonuclear dipolar coupled, and (iii) for either of these cases under magic-angle spinning (MAS) conditions. Herein, we demonstrate that short refocusing pulses that cause small flip angles can reduce the attenuation of signal in CPMG echo trains resulting from dipolar dephasing caused by the weak homonuclear dipolar couplings. For both spin-1/2 and quadrupolar nuclei, this can lead to significant extensions in $T_2^{\text{eff}}$ and signal enhancements of up to three times compared to conventional CPMG in favourable cases. These phenomena can occur under both static and magic-angle spinning (MAS) conditions, in the latter of which homonuclear couplings are reintroduced by rotational resonance ($R^2$) recoupling. Experimental examples of $^{13}$C ($I$ = 1/2), $^{2}$H ($I$ = 1), $^{87}$Rb ($I$ = 3/2), $^{23}$Na ($I$ = 3/2), and $^{35}$Cl ($I$ = 3/2) NMR under static and MAS conditions, as well as simulations of these phenomena, are shown and discussed.

**Keywords**: Solid-state NMR spectroscopy; CPMG; Homonuclear Dipolar Coupling; Rotational Resonance; Signal Enhancement

Journal Pre-proofs

## 1. Introduction

The Carr-Purcell/Meiboom-Gill (CPMG) pulse sequence was introduced for measuring transverse relaxation time constants ($T_2$),[1,2] and variants were later adapted for enhancing signal-to-noise ratios (SNR) in SSNMR experiments by Slichter and co-workers, who used these to acquire $^{17}$O, $^{89}$Y, and $^{13}$C SSNMR spectra.[3–5] The appropriate implementation of CPMG sequences for SNR enhancement was later found to depend on which NMR interaction(s) is(are) dominant in a given spin system, including the chemical shift anisotropy (CSA), the first- and/or second-order quadrupolar interactions (FOQI/SOQI), paramagnetic interactions, dipolar interactions, and any combination thereof. For instance, Bloom and Sternin, followed by Larsen and coworkers, developed the quadrupolar (Q)CPMG pulse sequence for efficient acquisition of SSNMR spectra of integer- and half-integer-spin nuclei,[6–9] the practical aspects of which are nicely detailed by Hung and Gan (particularly for wideline spectra).[10] Iijima and coworkers have demonstrated the use of a modified (Q)CPMG sequence for acquiring paramagnetically broadened $^{2}$H spectra.[11,12] Further explorations in this vein include those of O'Dell, Schurko, and co-workers, who introduced the WURST-CPMG pulse sequence for the efficient acquisition of wideline and ultra-wideline NMR spectra of both spin-1/2 and quadrupolar nuclei.[13–16] More recently, Grandinetti and coworkers demonstrated augmenting the *effective* $T_2$'s ($T_2^{\text{eff}}$, *vide infra*) of central transition (CT, +1/2 ↔ –1/2) powder patterns of half-integer spin quadrupolar nuclei by weak RF irradiation with CPMG.[17]

Direct dipolar interactions can significantly impact the implementation and performance of the CPMG pulse sequence. This impact can be determined from quantities that arise intrinsically from relaxation, such as the transverse relaxation time constant, $T_2$. The effective $T_2$ ($T_2^{\text{eff}}$) measured by CPMG sequences can also be impacted, which differs from the natural $T_2$

based on experimental conditions (*e.g.*, decoupling, finite pulse effects and imperfections, echo spacings, temperature effects, MAS,[18] magic-angle offsets, *etc*.). Moreover, there are phenomena that affect the broadening of spectral lines or powder patterns that also influence CPMG acquisitions that arise from wholly secular, non-relaxative effects, such as inhomogeneous broadening resulting from anisotropic NMR interactions and magnetic susceptibilities; these are generally classified as $T_2^*$ effects, or effective $T_2^*$ ($T_2^{*\text{eff}}$) effects, which can differ from $T_2$* effects, depending upon the experimental conditions (*e.g.,* field inhomogeneities, decoupling, MAS, *etc*.). Heteronuclear (*IS*) dipolar interactions (where *I* and *S* are the abundant and dilute nuclei, respectively) are known to impact both $T_2^*$ and $T_2$, the latter of which can reduce the number of spin echoes acquired in a CPMG echo train if there are significant contributions from heteronuclear dipolar relaxation mechanisms.[19,20] Heteronuclear dipolar decoupling is therefore often implemented with CPMG to minimize these contributions, thereby extending the $T_2^{\text{eff}}$ to allow for acquisitions of higher SNR spectra.[16,21–23] It has similarly been observed that homonuclear (*II* or *SS*) dipolar interactions can influence the $T_2$ behaviour observed with Hahn echo, CPMG, and other multiple-pulse sequences. These effects depend on homonuclear dipolar coupling being in the strong or weak regime, as defined by the chemical shift difference between the coupled spins being less or greater than the orientation-dependent dipolar coupling strength, respectively (*i.e.*, $\Delta\nu_{\text{iso}} \lesssim \nu_{\text{D}}$ or $\Delta\nu_{\text{iso}} \gg \nu_{\text{D}}$, respectively). For instance, it has been demonstrated that strong homonuclear dipolar decoupling can impact $T_2^{\text{eff}}$ and $T_2^{*\text{eff}}$ under static and MAS conditions with pulse sequences such as with WAHUHA, Lee Goldberg (LG) irradiation, DUMBO, and others.[24–27] It has also been demonstrated that Carr-Purcell or CPMG pulse sequences that use short $\theta_{\text{ref}} = 90°$ pulses, and more generally, arbitrarily small refocusing pulse flip angles, can extend $T_2^{\text{eff}}$ for spin-1/2 nuclei that experience strong homonuclear dipolar

couplings.[28–30] Depending on the flip angle and echo spacing, the $T_2^{eff}$ can be increased to a limit that approaches $T_{1\rho}$.[31–34] Siegel *et al*. demonstrated drastic signal enhancements in wideline spin-1/2 spectra acquired with CPMG using 90° refocusing pulses, which in part was accredited to reducing the effects of homonuclear dipolar coupling.[21,35] To date, the effects of weak homonuclear dipolar coupling in CPMG echo trains with short refocusing pulses has not been investigated for quadrupolar nuclei under static or MAS conditions..

MAS can average or remove the manifestation of the anisotropic broadening encoded by various NMR interactions such as CSA and dipolar coupling for achieving high spectral resolution. However, for homonuclear dipolar coupled spins, dipolar interactions can be reintroduced under certain conditions known as rotational resonance ($R^2$),[36–40] where the spinning rate, $\nu_{rot}$, matches an integer multiple of the isotropic shift difference between a spin pair as $\Delta\nu_{iso} = n\nu_{rot}$. Primary $R^2$ conditions occur for $n$ = 1,2; higher-order $n$ = 0 and $n > 2$ conditions can occur in the presence of CSA and quadrupolar interactions. For small molecules, the $n$ = 0 $R^2$ recoupling condition usually occurs between the spins of the same atomic site of neighboring molecules.[41,42] The following studies outline important examples and first discoveries of such conditions. Gan and Robyr have described the spin diffusion for spin-1 $^2$H nuclei enhanced by the $n$ = 0 $R^2$ recoupling.[43] Kwak *et al.* have described the $n$ = 0 $R^2$ phenomenon that can occur between the CT and ST for half-integer spin nuclei. The recoupling to the ST is highly sensitive to the magic-angle setting which induces intriguing magic-angle effects on the $T_1$ measured by inversion recovery and the measured $T_2^{eff}$.[44,45] Finally, Edén and Frydman have also detailed $R^2$ mechanisms for half-integer spin quadrupolar nuclei.[40,46]

Herein, we discuss the impact of weak homonuclear dipolar couplings on the $T_2^{eff}$-weighted decay of CPMG echo trains and concomitant spectra acquired with CPMG pulse

sequences for spin-1/2 and quadrupolar nuclei. This weak homonuclear coupling effect is often significant for small molecules with abundant high-γ nuclei; however, some other cases with moderate abundances and/or moderate-to-low values of γ are also explored. It is shown that short refocusing pulses can reduce the effects of the homonuclear dipolar interaction on the echo train and make the $T_2^{eff}$ longer, which leads to an overall signal enhancement in the resulting NMR spectra (this effect occurs to a degree outweighing the reduced efficiencies of shorter refocusing pulses). Several experimental examples are showcased, including $^{13}C$ ($I = 1/2$), $^{2}H$ ($I = 1$), $^{87}Rb$ ($I = 3/2$), $^{23}Na$ ($I = 3/2$), and $^{35}Cl$ ($I = 3/2$) NMR under static and MAS conditions. Numerical simulations of model spin systems provide insight to the underlying mechanisms and spin dynamics.

## 2. Experimental

### *2.1 Samples*

Partially-deuterated α-glycine [α-glycine-$d_2$, Cambridge Isotope Laboratories, Inc.], urea-$d_4$ [Sigma Aldrich], 1,8-dimethylnapthelene-$d_{12}$ [Cambridge Isotope Laboratories, Inc.], 1,2-phthalic anhydride-$^{13}C_2$ [Sigma Aldrich], rubidium nitrate [$RbNO_3$, Sigma Aldrich], sodium sulfate [$Na_2SO_4$, Sigma Aldrich], L-histidine hydrochloride monohydrate [L-Histidine HCl□$H_2O$, MP Biomedicals, LLC] were purchased, and deuterated MIL-53(Al)-$d_4$ was synthesized according to the literature.[47,48] Benzoic acid and dimedone were purchased and then deuterated by ball milling with $D_2O$ to produce benzoic acid-*d* and dimedone-*d*, respectively. The identities and purities of the samples were verified through comparisons with previously reported NMR spectra and PXRD patterns.[48,49] All samples were ground into fine powders and packed into 3.2 mm rotors or 5 mm outer-diameter glass tubes that were sealed with Teflon tape.

*2.2 Solid-State NMR Spectroscopy*

NMR spectra were acquired using a Bruker Avance NEO console and a 14.1 T Magnex/Bruker ($\upsilon_0(^1H)$ = 600 MHz) wide-bore magnet at resonance frequencies of $\upsilon_0(^2H)$ = 92.104 MHz, $\upsilon_0(^{23}Na)$ = 158.730 MHz, $\upsilon_0(^{35}Cl)$ = 58.792 MHz, and $\upsilon_0(^{87}Rb)$ = 196.348 MHz, and using a Bruker Avance NEO console with a 18.8 T Oxford ($\upsilon_0(^1H)$ = 800 MHz) medium-bore magnet at a resonance frequency $\upsilon_0(^{13}C)$ = 201.096 MHz. A home-built 5 mm double-resonance (HX) static probe was used for static $^2H$ experiments at 14.1 T, a home-built 3.2 mm triple resonance (HXY) magic-angle spinning (MAS) probe was used for $^{23}Na$, $^{87}Rb$, and $^{35}Cl$ experiments at 14.1 T, and a home-built 3.2 mm HXY MAS probe was used for $^1H$-$^{13}C$ experiments at 18.8 T. Spectra were acquired with $^1H$ continuous-wave (CW) decoupling with RF fields of 50 kHz for compounds having protons. RF pulse powers and chemical-shift reference frequencies were calibrated using the following standards: $^2H$ reference: $D_2O$ (*l*) with $\delta_{iso}$ = 4.8 ppm; $^{13}C$ reference: $^{13}C$-glycine (*s*) with $\delta_{iso}$ = 176.5 ppm; and the following were only used as chemical-shift references: $^{87}Rb$ reference: 0.1 M RbCl in $D_2O$ (*aq*) with $\delta_{iso}$ = 0.0 ppm; $^{23}Na$ reference: 0.1 M NaCl in $D_2O$ (*aq*) with $\delta_{iso}$ = 0.0 ppm; $^{35}Cl$ reference: NaCl (s) with $\delta_{iso}$ = 0.0 ppm. $^{23}Na$, $^{87}Rb$, and $^{35}Cl$ RF pulse powers were calibrated by finding the main spin-lock rotary resonance conditions, $(S+1/2)\nu_1 = \nu_{rot}$,[50,51] at $\nu_{rot}$ = 5 kHz and 10 kHz with $Na_2SO_4$, $RbNO_3$, and Histidine HCl□$H_2O$, respectively.

*2.3 Simulations*

All numerical spin-density matrix simulations were conducted in SIMPSON 4.2.1 using either 4180 or 28656 orientations sampled according to the ZCW averaging scheme.[52,53]

Simulations with dipolar couplings use two spins with a single dipolar coupling between them. CPMG pulse sequences are simulated using 32 spin echoes in all cases. All calculations were performed on a PC operating with Windows 10 using an Intel i9-9920X CPU.

## 3. Results and Discussion

### *3.1 Pulse Sequence Considerations and Overview*

The optimal implementations of the spin-echo and/or CPMG pulse sequences depend on what NMR interactions are dominant in the observed system. The sequence is typically initiated with an excitation pulse with a flip angle $\theta_{exc} = 360\nu_1\tau_{exc}$ (in degrees) of 90° (in the case of half-integer quadrupolar nuclei, a CT-selective excitation pulse is used, $\theta_{exc}^{sel} = \theta_{exc}/(I + 1/2)$).[54,55] The refocusing pulse has a flip angle, $\theta_{ref}$, that depends upon which NMR interactions are being refocused (**Figure S1**, N.B.: the same refocusing pulse is used repeatedly within the CPMG train). For spin interactions with a linear operator of the observed spin [*e.g.,* CSA, paramagnetic broadening, and/or SOQI (when $\nu_Q \gg \nu_1$)], $\theta_{ref} = 180°$ (or CT selective, $\theta_{ref}^{sel} = 180°/(I + 1/2)$) optimally refocuses the evolution of the isochromats evolving under these interactions to form the spin echo (this is most commonly referred to as the Hahn-echo pulse sequence). For spin interaction with traceless bilinear spin operators (*e.g.,* homonuclear dipole-dipole and FOQI), $\theta_{ref} = 90°$ is optimal; these are often referred to as a solid- and quadrupolar-echo sequences, respectively. For simplicity, θ is used herein to refer to the refocusing pulse flip angle, unless otherwise stated. In the above cases, if a small θ (*i.e.* $\theta < 180°$ or $< 90°$ for linear or bilinear interactions, respectively) is used, it generates an effective rotation axis ($B_{1,eff}$) that deviates from the direction of $B_1$ for the refocusing of spin polarization, resulting in a reduced projection of spin polarization in the *xy*-plane of the rotating frame.[56,57] If these small θ refocusing pulses are

used, by shortening the pulse width and fixing the RF amplitude, that results in reduced signal intensity, but has the added benefit of increased refocusing bandwidth, which is useful for wideline or ultra-wideline systems.[10,58] The total sensitivity gain afforded from CPMG also strongly depends on the decay of the echo train (*i,e.* $T_2^{eff}$), where long $T_2^{eff}$'s allow for the acquisition of many spin echoes, resulting in increased SNR. In this study, we will show that for various spin systems with weak homonuclear dipolar couplings that CPMG pulse sequences using small-θ refocusing pulses can prolong the decay of the echo-train (*i.e.*, increased $T_2^{eff}$). The signal gain from increased $T_2^{eff}$ can often outweigh the reduction in signal arising from decreased pulse sequence efficiency, resulting in an enhancement of overall SNR for CPMG spectra.

We will consider homonuclear dipolar coupling in two regimes: strong coupling and weak coupling, which are defined as cases where the shift differences between coupled spins are smaller or larger than the dipolar coupling strength, respectively. For strong homonuclear dipolar coupling, such as that between protons in diamagnetic solids, the chemical shift differences are almost always much smaller than typical $^1$H-$^1$H dipolar couplings. The terms of the homonuclear dipolar Hamiltonian that yield secular effects in spectra include the dipolar order ($S_{jz}S_{kz}$) and flip-flop ($S_{j+}S_{k-} + S_{j-}S_{k+}$) terms, which are written together as $3S_{jz}S_{kz} - (S_{jx}S_{kx} + S_{jy}S_{ky})$ (where $j$ and $k$ are the unique spin labels). 90° excitation and refocusing pulses effectively toggle the rotating frames in the spin-space among the *x*-, *y*-, and *z*-axes. The toggling frames effectively average the effects of the homonuclear dipolar Hamiltonian, achieving the well-known solid-echo and homonuclear dipolar decoupling.[24,59,60] Similar solid echoes can be obtained in CPMG sequences employing 90° refocusing pulses; however, these echoes usually decay very quickly, especially for cases of narrow peaks/patterns, which require long echo windows. Usually, refocusing pulses used with very short echo windows are referred to as pulsed spin-lock sequences instead of

CPMG.[61,62] For this reason, we do not consider the case of strong dipolar coupling herein (*e.g.*, large $^{1}$H-$^{1}$H couplings in diamagnetic solids). The homonuclear dipolar interactions considered in this work are in the weak coupling regime. Hence, the flip-flop terms can be truncated by the secular approximation, due to the much larger shift differences among the spins.[63,64] As such, it is sufficient for us to consider only the $3S_{jz}S_{kz}$ terms for weak homonuclear dipolar interactions.

We consider the weak homonuclear coupling a bilinear interaction. When pulses are applied to a homonuclear spin pair, the RF acts on both spins, which is distinct from the cases of chemical shift and heteronuclear spin interactions where it acts on only one spin. Thus, the inversion of spin operators by an ideal refocusing pulse does not lead to the sign change of the density matrix influenced by the homonuclear spin Hamiltonian. It is well-known in solution-state NMR that homonuclear *J*-couplings modulate spin echoes, and their effects are not refocused by the Hahn-echo pulse sequence.[65,66] These concepts can be extended to the behavior of spins subjected to repeated refocusing pulses used in CPMG experiments; from this, we can understand how weak homonuclear dipolar couplings affect the $T_2^{\text{eff}}$ and concomitant echo-train decay.

Herein, we explore how the weak homonuclear dipolar interaction manifests in CPMG echo trains and their corresponding spectra based on different refocusing pulse angles. Consideration is given to spin systems having a dominant linear (*i.e.*, CSA, SOQI) or traceless bilinear (*i.e.*, FOQI) interaction, along with weak homonuclear (*S*-*S*) dipolar coupling interactions. When refocusing pulses shorter than the standard $\theta = 180°$ (for dominant linear interactions) or $\theta = 90°$ (for traceless bilinear interactions) are used, respectively, the *S*-*S* dipolar dephasing is partially attenuated. This effect can be understood by consideration of the θ-REDOR pulse sequence and its application to heteronuclear (*S*-*I*) dipolar coupled systems, where

the refocusing of one of the heteronuclear spin pairs can be changed arbitrarily while others are kept at the ideal refocusing condition. Reducing the fraction of the spin states with heteronuclear coupled *I* spins with a $\theta < 180°$ pulse on the *I*-channel minimizes the number of *I* spins contributing to the dipolar dephasing of the *S* signal.[67] Smaller values of θ result in reduced contributions from the coupled *I* spins to dipolar dephasing/modulations that impact echo refocusing and formation. These effects are also exploited in SECSY, E-COSY, and bilinear-COSY pulse sequences that use small θ-refocusing pulses to minimize the evolution of spin polarization under bilinear *J*-coupling terms.[68–71] It may be possible to exploit this phenomenon to reduce the attenuation of the transverse spin polarization under weak homonuclear dipolar coupling in CPMG echo trains with small θ-refocusing pulses, while simultaneously refocusing transverse spin polarization evolving under the dominant anisotropic NMR interaction.

In the following sections, we describe the use of CPMG or CP-CPMG pulse sequences under static and MAS conditions with a fixed RF amplitude $\nu_1$ for excitation and refocusing pulses (unless otherwise stated), where the excitation pulse width, $\tau_{exc}$, is fixed (**Figure S1**). In experiments and simulations, the refocusing pulse width, $\tau_{ref}$, is arrayed such that the refocusing flip angle, $\theta = 360\nu_1\tau_{ref}$ (in degrees), changes accordingly; the resulting FIDs, powder patterns, and integrated pattern areas are compared. Practical guidelines for implementing these sequences, based on all of our findings, are presented in Section 3.5. Herein, it is shown that in the presence of weak homonuclear dipolar interactions, small flip angles resulting from short refocusing pulses reduce the dephasing effects of homonuclear dipolar interactions in CPMG echo trains, leading to increased values of $T_2^{eff}$ and concomitant signal enhancement in comparison to conventional refocusing flip angles. It is observed that the signal enhancements and optimal θ values vary between individual samples based on their homonuclear dipolar



Journal Pre-proofs

constants, intrinsic $T_2$'s, and other factors. Experimental $^{13}C$ ($I = 1/2$), $^{2}H$ ($I = 1$), $^{87}Rb$ ($I = 3/2$), $^{23}Na$ ($I = 3/2$), and $^{35}Cl$ ($I = 3/2$) NMR and spin-density matrix simulations are discussed.

*3.2 $^{13}C$ SSNMR Experiments*

The static $^{1}H$-$^{13}C$ CP-CPMG NMR spectra (**Figure 1**) of isotopically enriched 1,2-phthalic anhydride-$^{13}C_2$ feature a wideline pattern that is primarily influenced by a large CSA, as well as significant contributions from homonuclear dipolar broadening due to the short $^{13}C$-$^{13}C$ bond (the dipolar coupling, $\nu_D \approx 2790$ Hz).[72] This sample is ideal for testing the effects of weak homonuclear dipolar coupling on CPMG echo trains, since it is isotopically enriched and approximates an isolated homonuclear spin pair; therefore, we anticipate the observation of significant effects from the dipolar coupling. The two $^{13}C$-labeled sites are magnetically non-equivalent in the solid state, with $\delta_{33}$ oriented orthogonally to the ring plane, and $\delta_{22}$ tilted by an azimuthal angle of $\alpha = 24°$ from the C-C bond;[72] however, a better fit of the spectra acquired at a higher magnetic field is obtained in the current work using $\alpha = 35°$ (**Figure S2**). Initial CPMG experiments feature different flip angles for refocusing pulses, initially under static conditions, to see which values of $\theta$ lead to powder patterns having uniform appearance and maximal integrated area. After the CP contact period and echo delay time, a CPMG pulse sequence employing refocusing pulses with RF amplitudes of 100 kHz are used, where the refocusing pulse width, $\tau_{ref}$, is varied from $\tau_{ref} = 5$ μs ($\theta = 180°$) to $\tau_{ref} = 1.25$ μs ($\theta = 45°$) (**Figure 1**). In each experiment, the time-domain CPMG echo train is recorded, from which the $T_2^{eff}$ is measured, and subsequent echo coaddition and Fourier transform give the corresponding $^{13}C$ powder pattern. The pattern areas are measured by integration and compared to that of the $\tau_{ref} = 5$ μs ($\theta = 180°$) experiment, which is normalized to 1.00 (**Figure 1a**). Echo trains are fit with a

monoexponential decay function of the form $a \cdot \exp[-\tau/T_2^{eff}]$ to approximately measure the differences in effective coherence lifetimes between experiments; however, the echo trains will simultaneously encode oscillations originating from anisotropic dipolar couplings and these effects are not included in the fit for simplicity. For example, in the $\tau_{ref}$ = 5 μs (θ = 180°) experiment (**Figure 1a**), the echo train features echoes of varying intensity that oscillate between relatively low and high signal intensities. The corresponding powder pattern is distorted and does not resemble a typical $^{13}C$ CSA or dipolar pattern. As $\tau_{ref}$ decreases from 5 μs, corresponding to smaller flip angles, the powder pattern area increases, until a maximum is reached at $\tau_{ref}$ = 2.5 μs (90°); at this point, a 3.2-fold increase in area is observed, and the powder pattern resembles that in a conventional CSA and dipolar-broadened spectrum (**Figure 1d**). After this point, the area decreases for shorter pulse widths. The $T_2^{eff}$ also increases with respect to that of $\tau_{ref}$ = 5 μs (θ = 180°) when using a shorter $\tau_{ref}$ and is maximized when using $\tau_{ref}$ = 1.25 μs (θ = 45°), whereas pattern area is maximized with $\tau_{ref}$ = 2.5 μs (θ = 90°).[56,57] It is difficult to accurately quantify $T_2^{eff}$ in this case since the dipolar oscillations are not included in the fit, however these experiments may be useful in extracting information on the dipolar coupling.[67,73] Regardless of the $\tau_{ref}$ used, the second echo in the CPMG train is never fully formed, likely to residual dipolar oscillations; therefore, that echo is not included for $T_2^{eff}$ fits. Small θ < 180° refocusing pulses encode less dipolar oscillations in the CPMG echo trains where the envelope of the train becomes more monoexponential with decreasing θ; however, the dipolar oscillations cannot be fully removed when using a small θ.[30]

180° refocusing pulses would be expected to optimally refocus isochromats evolving under the influence of the CSA in the absence of any other interactions. However, an increased $T_2^{eff}$ and signal enhancement is obtained around $\tau_{ref}$ = 2.5 μs (90°) in comparison to the $\tau_{ref}$ = 5.0

μs (180°) experiment (**Figure 1**). As described above, values of θ that are < 180° will reduce the dipolar dephasing in cases where the *S*-*S* coupled spins evolve under a weak homonuclear dipolar coupling interaction, which for CPMG pulse sequences, leads to increased pattern areas and longer measured values of $T_2^{eff}$. These results suggest a balance needs to be struck between reducing the homonuclear dipolar dephasing via the use of small θ refocusing pulses (< 180°) that allow for the acquisition of more spin echoes, while also causing minimal losses from the sub-optimal refocusing of the spin polarization evolving under the influence of CSA. The optimal value of θ that is required to achieve this balance varies between spin systems, and can depend on the relative size of the homonuclear dipolar coupling constant(s), the number of coupled spins, relative CS and dipolar tensor orientations, and the intrinsic $T_2$ of the system.

The effects of homonuclear dipolar coupling are further explored using numerical simulations of experiments using a CPMG pulse sequence with maximum RF amplitude of 100 kHz, $\tau_{exc}$ = 2.5 μs (90°), and $\tau_{ref}$ varied between 5 μs and 0.5 μs. The AB spin system consists of the two magnetically non-equivalent $^{13}C$ spin CS tensors that only differ by the orientation of their $\delta_{11}$ and $\delta_{22}$ components (*vide supra* and **Figure S2**) and features an array of dipolar coupling constants, $\nu_D$. The resulting contour plot shows a maximum powder pattern area, as indicated by the intensity (in arbitrary units), for $\nu_D$ = 0 Hz and $\tau_{ref}$ = 5.0 μs (180°) (**Figure 2a**), consistent with refocusing of isochromats in a CSA-dominated pattern. When $\nu_D \gtrsim 100$ Hz, maximum pattern area is observed for cases with $\tau_{ref}$ = 2.5 μs (90°), whereas cases with $\tau_{ref}$ = 5.0 μs (180°) are found to have lower relative areas. Examples of the FIDs and spectra are shown for the case of two overlapping CSA powder patterns with $\nu_D$ = 0 Hz (**Figure 2b**, **2c**). Maximum area (1.0) is observed for $\tau_{ref}$ = 5.0 μs (180°) pulses (**Figure 2b**), and a reduction by a factor of $1/\sqrt{2}$ is observed for $\tau_{ref}$ = 2.5 μs (90°) pulses (*i.e.*, the projection of spin polarization into the *xy*-

plane is scaled by cos(45°) = 0.71) (**Figure 2c**). When the homonuclear dipolar coupling of $\nu_D$ = 2790 Hz is used in the simulation, 180° refocusing pulses perform poorly, yielding a spectrum with a non-uniform pattern (**Figure 2d**). By comparison, 90° refocusing pulses yield a spectrum with a large signal enhancement relative to the 180° pulses and matches well with the experimental result (**Figure 2e**, *cf*. **Figure 1d**). It may be difficult to quantitatively replicate experimental conditions and results since intrinsic $T_2$'s or $T_2^{eff}$'s cannot be included in numerical simulations in SIMPSON, and potential longer-range, intermolecular couplings are not considered.

MAS is widely used in SSNMR for averaging the manifestation of second-rank anisotropic spin interactions such as CSA, leading to high-resolution NMR spectra with isotropic chemical shifts in some cases. When the spinning rate (in Hz) is smaller or on the order of the anisotropy, spinning sideband (SSB) manifolds are observed with envelopes that somewhat resemble the static CSA powder patterns.[74,75] For strongly coupled spin systems, such as those with many homonuclear dipolar coupled protons, MAS only averages the effects of dipolar coupling to first order. Residual line widths under MAS from higher orders are highly sensitive to spinning speed.[76–78] For weakly coupled spins, the degree to which MAS averages the dipolar coupling is highly dependent on the isotropic shift difference between the two spins, which can cause $R^2$ recoupling (*vide supra*).

The two labeled sites of 1,2-phthalic anhydride-$^{13}C_2$ have the same isotropic chemical shift, meeting the requirement for the $n = 0$ $R^2$ condition, since they are rendered magnetically distinct from one another due to their distinct CS tensor orientations. High-resolution CP/MAS spectra are used to observe the $R^2$ recoupling, then CP-CPMG/MAS is used to test dipolar coupling effects on CPMG echo trains. The effects of homonuclear dipolar recoupling are clearly

noticeable in $^{1}H$-$^{13}C$ CP/MAS NMR spectra acquired at spinning frequencies of 3 and 5 kHz (**Figure 3a**, **3b**); we note that the $n = 0$ $R^2$ condition is always satisfied independent of the spinning speed, though the magnitude of the recoupled interaction depends on the spinning speed, as indicated by the splittings in the spinning sidebands (SSBs). The effects of recoupling become smaller than the SSB linewidth at $\nu_{rot} = 10$ kHz (**Figure 3c**). Substantial effects from the homonuclear dipolar coupling are also observed in $^{1}H$-$^{13}C$ CP-CPMG/MAS NMR spectra acquired at $\nu_{rot} = 5$ kHz (**Figure 4a**, **4b**) and 3 kHz (**Figure 4c**, **4d**). The dipolar splittings in the SSB's are present in these CPMG spectra, but less resolved in comparison to those in spectra acquired with conventional $^{1}H$-$^{13}C$ CP/MAS, due to both reduced resolution from windowed acquisition during CPMG that maximizes the number of echoes and the application of Gaussian line broadening that attenuates sinc artifacts.

At both spinning frequencies, significant signal enhancements resulting from reduced dipolar dephasing and concomitant increases in $T_2^{eff}$ occur for experiments implementing $\tau_{ref} = 2.5$ μs (90°) in comparison to those employing $\tau_{ref} = 5.0$ μs (180°) (**Figure 4**). This enhancement is much smaller than the static case, though this is to be expected since the effective $\nu_D$ (*i.e.*, $\nu_D^{eff}$) under MAS is reduced in comparison to the $\nu_D$ under static conditions. Significant oscillations in the echo trains are still evident at both spinning frequencies for $\tau_{ref} = 5$ μs (180°) (**Figure 4a**, **4c**) and are significantly attenuated with $\tau_{ref} = 2.5$ μs (90°) (**Figure 4b**, **4d**), just like the static case. On a side note, we did not observe analogous homonuclear dipolar coupling effects in our previous study featuring CPMG-MAS NMR experiments on spin-1/2 nuclei such as $^{119}Sn$ (n.a. = 8.6 %), $^{195}Pt$ (n.a. = 33.8 %), and $^{207}Pb$ (n.a. = 22.1 %); this is likely due to both a reduced number of homonuclear dipolar couplings and smaller $\nu_D^{eff}$ arising from the combination of lower natural abundances of these isotopes and increased nuclear distances.[58] In addition,

homonuclear coupling by the $n = 0$ $R^2$ condition requires frequency differences arising from the CSA, the contributions of which to the powder pattern are is modulated by MAS.[51] Observations of augmented $T_2^{eff}$'s similar to those reported in the current work were reported by Cowans and Grutzner for rotor-synchronized $^1$H-$^{13}$C CP-CPMG experiments in which different composite pulse widths for refocusing were compared;[79] however, the effects of homonuclear dipolar couplings were not discussed. More detailed analyses of dipolar effects in CPMG echo trains were described by Barret *et al.*, but consideration was not given to the effect of variable flip angles used in the CPMG pulse sequence.[80–82]

*3.3 $^2$H Experiments*

Consideration is now given to the performance of (Q)CPMG pulse sequences on $^2$H nuclei that experience weak homonuclear dipolar couplings and have powder patterns that are influenced by substantial FOQI broadening. It is well known that $\theta = 90°$ refocusing pulses in (Q)CPMG pulse sequences refocus the spin polarization influenced by the FOQI,[6–9] and when simultaneous paramagnetic or CSA interactions are present, a combination of interleaved $\theta = 180°$ and $\theta = 90°$ can refocus both interactions;[11,12,83,84] however, the impact of weak $^2$H-$^2$H dipolar couplings has not been explored for CPMG sequences to date. Several samples featuring unique labeling schemes and concentrations, different sets of effective $^2$H-$^2$H distances ($r_D$), and therefore, unique sets of homonuclear dipolar coupling constants, were studied using (Q)CPMG pulse sequences (**Table I**, see the supporting information for figures of all of the echo trains and spectra, **Figure S3 – S7**). In every case, a maximum RF amplitude of 100 kHz is used for excitation and refocusing, $\tau_{exc} = 2.5$ μs, and $\tau_{ref}$ is varied between 2.5 μs (90°) and 0.75 μs (27°).

For each case, we report $T_2^{eff}$'s and the ratio of the powder pattern areas from the CPMG experiments using conventional 90° and θ < 90° refocusing pulses (**Table I**).

Different flip angles for refocusing pulses were first tested in a (Q)CPMG pulse sequence for $^2$H NMR of α-glycine-$d_2$ under static conditions (**Figure 5**). As $\tau_{ref}$ decreases from 2.5 μs, corresponding to smaller flip angles, the powder pattern area increases, until a maximum is reached at $\tau_{ref}$ = 1.25 μs (45°), for which a 1.9-fold increase in area is observed (**Figure 5f**). After this point, the area decreases with decreasing pulse widths. The corresponding SNR also increases for $\tau_{ref}$ = 1.25 μs (45°); however, SNR enhancement must be interpreted with caution since the maximum SNR depends on how many echoes are processed and SNR varies across an anisotropic powder pattern (**Figure S8**). Therefore, we measure area throughout this work for consistency. The $T_2^{eff}$ also increases with progressively shorter refocusing pulse widths. However, its maximum value is not observed for the pattern of maximum area; rather, it continues to increase with decreasing pulse widths (**Figure S9)**. Increased pattern area could potentially be obtained for $\tau_{ref}$ < 1.25 μs; however, the acquisition time is limited when high-power $^1$H decoupling is used, such as it is in the current example. The first echo in each CPMG train progressively loses intensity for decreasing $\tau_{ref}$ with respect to the first echo formed in the experiment using $\tau_{ref}$ = 2.5 μs (θ = 90°) and the second and third echoes continue to lose intensity below $\tau_{ref}$ = 1.25 μs (the reasons for this are explored with numerical simulations, *vide infra*); as such, the first three echoes are not included in the $T_2^{eff}$ fits for these reasons; however, all echoes are used for the Fourier transform. It is important to note that the significant increases in pattern area with θ < 90° are not a consequence of increased refocusing-pulse bandwidths, as can be readily observed by examining isochromat intensities around the transmitter (*i.e.*, 0 Hz offset).

In α-glycine-$d_2$, there is a short distance between the -$CD_2$ deuterons of $r_D$ = 1.817 Å, giving rise to a homonuclear dipolar coupling of $\nu_D$ = 472 Hz (**Table I**); to a good approximation, this system is regarded as having an isolated $^2$H-$^2$H spin pair, though there may be multiple, smaller intermolecular dipolar couplings. Small θ-refocusing pulses can attenuate dipolar dephasing significantly in the CPMG echo trains of $^2$H nuclei simultaneously influenced by the dominant bilinear FOQI and weak homonuclear dipolar couplings. These effects are further studied using both simulations and additional experiments on distinct spin systems that include varying numbers of homonuclear dipolar couplings of different magnitudes.

Numerical simulations of a CPMG pulse sequence were conducted for the $^2$H-$^2$H spin pair in α-glycine-$d_2$ using previously reported EFG tensor parameters.[85,86] The sequence uses a RF amplitude of 100 kHz and $\tau_{exc}$ = 2.5 μs with values of $\nu_D$ that vary between 0 and 1000 Hz and $\tau_{ref}$ that range from 2.5 μs to 0.75 μs. The resulting contour plot (**Figure 6a**) shows maximum pattern area at $\tau_{ref}$ = 2.5 μs (90°) for $\nu_D$ = 0 Hz, as would be expected for refocusing isochromats evolving solely under the FOQI. For $\nu_D \gtrsim 400$ Hz, local maxima are apparent at $\tau_{ref}$ = 1.5 μs (54°), whereas $\tau_{ref}$ = 2.5 μs (90°) yields less intensity by comparison, in relatively good agreement with experimentally observing maximum enhancement with$\tau_{ref}$ = 1.25 μs (45°). The simulated FID for $\nu_D$ = 0 Hz and $\tau_{ref}$ = 2.5 μs (90°) has an echo train with a relatively flat profile, since there is no $T_2$ decay included in SIMPSON simulations (**Figure 6b**). The simulated FID for $\nu_D$ = 0 Hz and $\tau_{ref}$ = 1.5 μs (54°) (**Figure 6c**) has an initial echo that is substantially less intense than the $\tau_{ref}$ = 2.5 μs (90°) case, which is a common observation for CPMG echo trains employing a small θ;[10,56] this effect can be further understood by considering initial zero-quantum coherence (ZQC) generation (*cf.* **Figure S10**). The experimental echo trains also show a loss of intensity in the first echo and increased $T_2^{eff}$ as the refocusing pulse width is decreased,

even below 1.5 and 1.25 μs (*cf*. **Figure 5e-h** and **Figure S9**). In simulations, the areas of the powder patterns for $\tau_{ref}$ = 1.5 μs (54°) are reduced with respect to that of $\tau_{ref}$ = 2.5 μs (90°) (*cf*. **Figure 6b, 6c**), which is consistent with 90° refocusing pulses as the best choice in quadrupolar-echo or QCPMG-type pulse sequences for optimal refocusing of isochromats evolving solely under the FOQI.[6,7,83]

Similar numerical calculations were carried out with $\nu_D$ = 450 kHz; FIDs and patterns for the $\tau_{ref}$ = 2.5 μs (90°) and $\tau_{ref}$ = 1.5 μs (54°) cases are shown in **Figure 6d** and **Figure 6e**, respectively. The magnitude of the echo train in the former case reveals an apparent oscillation that originates from the time-propagation of the homonuclear dipolar Hamiltonian. Interestingly, this oscillation effectively reduces the intensity of several spin echoes, especially those early in the echo train. In the latter case, this oscillation is attenuated, leading to higher overall signal in the echo train and powder pattern, as indicated by the normalized area (*cf*. **Figure 6d, 6e**). If refocusing pulses with θ < 90° are used in a CPMG experiment for spin-1 nuclei, the effects of the homonuclear dipolar coupling are reduced, leading to an increase in the measured value of $T_2^{eff}$ and pattern area. Again, quantitative simulated results are difficult to achieve since intrinsic $T_2$'s and potential intermolecular couplings are not considered, the latter of which may also affect the dipolar oscillations observed in simulations as compared to experiments.

We note that careful consideration must be given to the inter-echo delay, since this can also augment or reduce $T_2^{eff}$ for homonuclear dipolar coupled systems.[80–82,87] The windowed acquisition period (i) depends on the inter-echo delay and (ii) must be large enough to capture the entire echo. Therefore, it is recommended to use a fixed inter-echo delay time and use variable refocusing pulse widths, rather than varying echo delays, to increase $T_2^{eff}$'s in homonuclear dipolar coupled systems.

Additional samples, including urea-$d_4$ and 1,8-dimethylnapthelene (DMNAP)-$d_{12}$, both demonstrate a significant increase in the $T_2^{eff,45}$ in comparison to $T_2^{eff,90}$ (*i.e.,* the values of $T_2^{eff}$ measured with $\theta = 45°$ and 90°, respectively), as well as overall signal enhancements, likely owing to relatively strong homonuclear dipolar couplings in these systems (**Figures S3**, **S4**). In the case of DMNAP-$d_{12}$, the maximum enhancement is observed for a $\tau_{ref} = 1.0$ μs (36°) pulse (**Table I**). This difference may originate, in part, from its more complex homonuclear coupling behavior, since it is uniformly labeled and there are numerous intra- and intermolecular couplings between deuterons, as well as the differences in the intrinsic $T_2$'s of these systems[88] Nonetheless, the shorter refocusing pulse clearly augments the $T_2^{eff}$ and enhances signal with respect to conventional 90° refocusing pulses, consistent with our simulations on an isolated $^2$H-$^2$H spin pair.

Several samples, including benzoic acid-*d*, MIL-53-$d_4$, and dimedone-*d*, have smaller and/or fewer couplings; experiments analogous to those above reveal either a small $T_2^{eff}$ augmentation and/or signal enhancement, or a reduction of signal intensity (**Figures S5**, **S6**, and **S7**). The strongest coupling for benzoic acid-*d* is only slightly less than that of DMNAP-$d_{12}$, and yet, a reduction in signal intensity is observed when $\tau_{ref} = 1.25$ μs (45°) is used. Unlike DMNAP-$d_{12}$, with its multiple homonuclear dipolar couplings, benzoic acid-*d*, which forms a dimer in the solid state, is only labelled at the carboxylic acid site, and primarily appears as an isolated spin pair (AB system); this means that there is only a single homonuclear coupling in the latter case.[89] Furthermore, $^1$H decoupling with an RF field of 50 kHz is necessary for benzoic acid-*d*, which places restrictions on acquisition windows and decoupling fields (N.B.: $^1$H decoupling can also augment $T_2^{eff}$). Decoupling for acquisition periods longer than *ca*. 50 ms is not advisable due to limitations on the duty cycle of our probe. The use of $\tau_{ref} = 1.25$ μs (45°) extends the $T_2^{eff}$ decay

well beyond 50 ms, which may result in a net signal enhancement if those additional echoes are acquired; however, in the limited acquisition window, the shorter refocusing pulses yield a net decrease in signal. In addition, the H/D atoms of the carboxylic acid in the benzoic acid dimer undergo exchange, which may partially average the $^2$H-$^2$H dipolar coupling, resulting in a weaker effective coupling strength.[89,90] The $T_2^{eff}$ decay of MIL-53-$d_4$ is well within the sampling window and a small 1.08-fold signal enhancement is observed, likely owing to the relatively smaller $\nu_D$ = 208 Hz (**Figure S6**).[49] MIL-53-$d_4$ is also used to demonstrate that creating 45° refocusing-pulse nutation by fixing the pulse width at 2.5 μs and decreasing the RF amplitude to 50 kHz, yields a very similar result to adjusting the pulse width and fixing the amplitude. Finally, dimedone-*d* features the weakest coupling ($\nu_D$ = *ca.* 22 Hz) and signal is reduced from the application of shorter refocusing pulses (**Figure S7**). The $T_2^{eff}$ is somewhat enhanced with 45° refocusing pulses, but this is likely because of ZQC generation, as described in simulations (*vide supra*, **Figure S10**).

Final consideration is given to the previously reported signal enhancement for $^2$H NMR of α-glycine-$d_2$ under MAS conditions with the use of 45° refocusing pulses for CPMG that was conducted by our research group.[58] Gan and Robyr previously described homonuclear dipolar recoupling *via* a $n = 0$ $R^2$ condition for this sample under MAS because the two -$CD_2$ deuterons are non-equivalent due to different EFG tensor parameters and orientations.[43] Our previously reported experiments featured maximum RF amplitudes of 75 kHz, an $\tau_{exc}$ = 3.33 μs, and various refocusing pulse widths, where $\tau_{ref}$ = 1.67 μs corresponds to a 45° refocusing pulse in this case. Reexamining this data shows that the $T_2^{eff}$ under MAS is enhanced from 26.8 ms to 63.7 ms and the integrated area under the spinning side bands is enhanced by a factor of 1.17 (**Figure 7**). This enhancement factor is again smaller than that of the static case due to the reduced $\nu_D^{eff}$ under

MAS. The enhancement factor could be higher with the acquisition of more echoes since the $T_2^{eff}$ is longer; however, like in static experiments, one must be careful of using an acquisition time that is too long when high-power $^1$H decoupling is active. The same result is achieved using 45° refocusing pulses after a CP contact period in CP-CPMG/MAS.[58] It is anticipated that dipolar refocusing can be exploited for signal enhancement in other deuterated systems that experience homonuclear dipolar coupling under static and MAS conditions. This phenomenon may be potentially useful for distance measurements between deuterons.

*3.4 Experiments on Half-Integer Quadrupolar Nuclei*

We now consider the influence of weak homonuclear dipolar coupling in CPMG experiments on half-integer spin quadrupolar nuclei. Three different $I = 3/2$ cases are investigated, involving a range of distinct homonuclear dipolar coupling scenarios, including: (i) $^{87}$Rb (n.a. = 27.83%) of $RbNO_3$, with a moderate $\nu_D \approx 227$ Hz; (ii) $^{23}$Na (n.a. = 100%) of $Na_2SO_4$, with a moderate $\nu_D \approx 245$ Hz; and (iii) $^{35}$Cl (n.a. = 75.78%) of L-histidine HCl□$H_2O$, with a negligible $\nu_D \approx 6$ Hz. The values of $\nu_D$ listed above correspond to the shortest reported $r_D$, for simplification of comparing relative coupling strengths between compounds (**Table II**). We note that two of these systems, $RbNO_3$ and $Na_2SO_4$, also have extensive dipolar coupling networks, especially the latter (*vide infra*). For these nuclei, RF amplitudes of 10 kHz were used in CPMG pulse sequences with CT-selective pulse widths, where pulse widths of 25 μs and 12.5 μs cause CT-selective flip angles ($\theta_{sel}$) of 180° and 90°, respectively. In this section, the flip angles are always considered as CT selective, a $\tau_{exc} = 12.5$ μs (90°) is used for excitation, and various refocusing flip angles are tested. Numerical simulations are also presented for a generic case of a dipolar-coupled spin pair of $I = 3/2$ nuclei. These tests are distinct from the work of Grandinetti

*et al.*, where weak RF irradiation with fixed $\theta_{ref}^{sel} = 180°$ was used for substantial $T_2^{eff}$ enhancements as the result of excitation and refocusing that is highly selective to the CT and avoids any coherence loss to the satellite transitions (ST)s under MAS (*vide infra*).[17] Consideration is not given to the impact of residual dipolar coupling between quadrupolar nuclei under MAS in these cases.[40,91]

The first case is that of $^{87}$Rb NMR of $RbNO_3$, which based on internuclear $^{87}$Rb-$^{87}$Rb distances, is expected to have a maximum $\nu_D \approx 227$ Hz (**Table II**). Under static conditions, a large $T_2^{eff}$ enhancement and signal enhancement of 2.61 is observed in spectra acquired using $\theta_{ref}^{sel} = 90°$ in comparison to those acquired with $\theta_{ref}^{sel} = 180°$ (**Figure 8a**, **8b**). 90° refocusing pulses do not offer signal enhancement, likely due to spatiotemporal averaging of the dipolar interaction with $\nu_{rot} = 10$ kHz under MAS, resulting in signal loss of a *ca.* $1/\sqrt{2}$ (**Figure 8c**, **8d**). $RbNO_3$ has three sites with different shifts;[92–94] therefore, the $n = 0$ $R^2$ recoupling is much smaller among the non-equivalent sites, likely resulting in a negligible $\nu_D^{eff}$ at $\nu_{rot} = 10$ kHz. The corresponding $T_2^{eff}$ is moderately enhanced (**Figure 8d**) but is likely due to zero-quantum coherence (ZQC) generation (*i.e.,* prolonged signal decay by refocusing stimulated and spin echoes, *vide supra*; *c.f.* **Figure S10**)[56,95] and does not yield signal enhancement. $RbNO_3$ is not known to experience an effective dipolar coupling between $^{87}$Rb nuclei by $R^2$ recoupling alone at $\nu_{rot} = 10$ kHz.[94] In each case, the first two echoes are not included in the $T_2^{eff}$ fits, since they are not fully formed in **Figure 8b**, **8d** with $\theta_{ref}^{sel} = 90°$ and result in a non-exponential decay; hence, only the remaining echoes are considered, since they appear to undergo an exponential decay. Multiple refocusing pulse widths were tested under static and MAS conditions, which show local minima of signal intensity when using the pulse sequence with $\tau_{ref} = 25$ μs (180°) when

homonuclear dipolar coupling is present and small signal enhancements with different $\theta_{ref}^{sel} <$ 180° at $\nu_{rot}$ = 2 and 5 kHz (**Figure S11**).

The second case is $^{23}$Na NMR of $Na_2SO_4$, which was chosen due to the multiple couplings of $^{23}$Na nuclei with close proximities (**Table II**), n.a. = 100 %, having five magnetically inequivalent sites, and previously reported evidence of the detection of effective dipolar coupling under MAS by $n$ = 0 $R^2$ recoupling since there are no shifts amongst the sites.[44,96–98] Like the case of $^{87}$Rb NMR, the static $^{23}$Na CPMG experiment shows maximum signal enhancement with $\tau_{ref} < 25$ μs; however, unlike the $^{87}$Rb case, this occurs for $\tau_{ref}$ = 10.0 μs (72°) with a 2.95-fold enhancement (**Figure 9a**, **9b** and **Figure S12**). Under MAS with $\nu_{rot}$ = 10 kHz, the $T_2^{eff}$ is increased from 8.15 ms to 22.47 ms and a maximum signal enhancement of 2.44 is achieved with $\tau_{ref}$ = 12.5 μs (90°) (**Figure 9c**, **9d** and **Figure S12**). This is in contrast to the $^{87}$Rb NMR case, as the homonuclear dipolar coupling between $^{23}$Na nuclei is recoupled under MAS at $\nu_{rot}$ = 10 kHz for this sample.[44]

The final case is that of $^{35}$Cl NMR of L-histidine HCl□$H_2O$, which features a single $^{35}$Cl chemically distinct site and four magnetically inequivalent sites (assuming non-negligible dipolar couplings between $^{35}$Cl nuclei),[99] was chosen with the anticipation that this homonuclear dipolar refocusing effect may not be observed for a $^{35}$Cl spin pair, due to the much lower gyromagnetic ratio of $^{35}$Cl (in comparison to those of $^{87}$Rb and $^{23}$Na) and their increased spatial separation (in this compound, $\nu_D \approx 6$ Hz) (**Table II**). Crucially, in a pulse width array under static conditions, a local minimum in signal intensity is observed with $\theta_{ref}^{sel}$ = 180°, whereas the same array under MAS with $\nu_{rot}$ = 10 kHz yields a maximum with $\theta_{ref}^{sel}$ = 180° (**Figure S13**), similar to the characteristic arrays observed in $^{87}$Rb and $^{23}$Na experiments (**Figures S11 and S12**). A longer $T_2^{eff}$ and slight increase in the maximum pattern area are observed for $\tau_{ref}$ = 20 μs (144°)

refocusing under static conditions (**Figure 10a, 10b**) but not under MAS (**Figure 10c, 10d**). The former result is surprising, as a depletion in signal intensity would be expected with $\theta_{ref}^{sel} < 180°$ for a spin pair solely influenced by the SOQI when the dipolar coupling constant is nearly negligible; hence, we investigated this further with numerical simulations.

The effects of homonuclear dipolar coupling on CPMG echo trains are examined for $I$ = 3/2 nuclei with numerical simulations using a spin system comprised of two equivalent $^{23}$Na spins with the same EFG tensor parameters as $Na_2SO_4$, with the largest component of their EFG tensors oriented at $\beta = 90°$ with respect to the internuclear vector. Multiple orientations between the two EFG tensors and between the EFG and dipolar tensors were tested, which had little impact on the simulated results. The impacts of different dipolar couplings and refocusing pulses (that vary from 50 to 2.5 μs, where $\tau_{ref}$ = 25 μs is a 180° refocusing pulse) on signal intensity are probed (**Figure 11a**). For $\nu_D = 0$ Hz, a maximum pattern area is observed for $\tau_{ref}$ = 25 μs (180°); however, $\nu_D > 0$ Hz and $\tau_{ref}$ = 25 μs (180°) results in local minima in pattern areas, even for small $\nu_D \sim 5$ Hz. For $\nu_D \geq 50$ Hz, maximum signal intensities are observed for $\tau_{ref}$ = 15 or 17.5 μs, depending on the magnitude of $\nu_D$. Some examples of FIDs and spectra for $\nu_D = 0$ Hz (**Figure 11b, c**) demonstrate that $\tau_{ref}$ = 25 μs (180°) refocusing pulses again perform best. When $\nu_D$ = 250 Hz, some dipolar splittings are observed in the static pattern that do not completely match the static experimental $^{23}$Na powder pattern (**Figure 11d, e**); this is due to our simulations involving only two spins, whereas the multiple homonuclear dipolar couplings in $Na_2SO_4$ exert a distinct influence on the appearance of the experimental powder patterns (*cf*. **Figure 9a**, **b**).[97] $\tau_{ref}$ = 15 μs (108°) now offers a signal enhancement in comparison to $\tau_{ref}$ = 25 μs (180°), which generally supports the hypothesis that shorter refocusing pulses yield uniform patterns of maximum areas in $^{87}$Rb and $^{23}$Na static experiments and $^{23}$Na MAS experiments where homonuclear dipolar

recoupling manifests. Simulations predict maximum signal enhancement for $\tau_{ref}$ = 20 μs (144°) when $\nu_D$ = 5 Hz for this spin system, which may explain the current experimental $^{35}$Cl observations and previous observations of SNR enhancement with $\theta_{ref}^{sel} < 180°$ in $^{35}$Cl NMR of $Cp_2ZrCl_2$.[10] These results suggest the possibility of probing distance measurements for a wide array of quadrupolar nuclei, particularly for cases of isolated spin pairs.

It is important to note that the mechanism for signal enhancement observed for half-integer quadrupolar nuclei in this work is not a consequence of the refocusing pulses with low RF amplitudes, as described by Grandinetti *et al.*[17] In their work, increases in $T_2^{eff}$ are observed in $^{17}$O and $^{33}$S CPMG/MAS spectra acquired with low-power (highly selective) refocusing pulses that are applied with a fixed $\theta_{ref}^{sel} = 180°$; corresponding enhancements are the result of avoiding coherence exchange with the STs by being highly selective for the CT. In the current work, $\nu_1$ is instead fixed and $\tau_{ref}$ and $\theta_{ref}^{sel}$ are varied, leading to increased pattern areas and $T_2^{eff}$'s, arising from reduced contributions of homonuclear dipolar dephasing. Furthermore, enhancements are observed under both MAS and static conditions, the latter of which minimize coherence exchanges between the CT and STs.[100]

*3.5 Practical Guidelines*

The following guidelines are recommended for the practical implementation of CPMG for systems with SSNMR spectra that experience weak homonuclear dipolar coupling:

1. The CPMG pulse sequence should be initiated with a 90° excitation pulse and the flip angle of the refocusing pulse, θ, should be arrayed either by (i) varying the pulse width with a fixed amplitude or by (ii) varying the pulse amplitude with a fixed width until the powder pattern area is maximized; however, the former is a more robust approach since this maximizes

refocusing bandwidth.[58] The optimal θ that maximizes SNR varies between samples and can depend on factors such as intrinsic $T_2$ differences between samples, MAS spinning speeds, the number of homonuclear dipolar couplings between nuclei and their strengths, relative EFG or CS and dipolar tensor orientations, and accurate MAS settings for half-integer spin quadrupolar nuclei. Therefore, θ will likely vary between systems even when identical nuclei are being probed, but the examples covered in this work reflect sensible starting points and ranges of conditions to test.

2. For experiments under MAS, rotor-synchronization should be maintained using previously outlined conditions,[58] and consideration should be given to the possibility of the occurrence of $R^2$ recoupling that can allow homonuclear dipolar coupling effects to manifest.

3. (a) For systems that are primarily influenced by linear interactions, including CSA, paramagnetic broadening, and/or SOQI and are simultaneously influenced by weak homonuclear dipolar couplings, the optimal $\theta < 180°$ (including the CT selective $\theta_{sel}$ when $\nu_Q > \nu_1$). (b) For analogous systems where the dominant interaction is instead traceless and bilinear (*i.e.,* the FOQI where off-resonance effects are neglected) the optimal $\theta < 90°$.

4. Careful consideration should be given to measured $T_2^{eff}$ exponential decay constants in systems that experience weak dipolar coupling, and their significance should be interpreted with caution. The envelope of the echo train will simultaneously encode an exponential decay and oscillations from the dipolar coupling, the latter of which are anisotropic under static conditions. The choice of refocusing pulse flip angle and the echo delay time can affect the measured $T_2^{eff}$ and how the dipolar oscillations manifest.

## 4. Conclusions

CPMG-type pulse sequences that use short refocusing pulses with small θ flip angles can yield substantial signal enhancements in SSNMR spectra of weakly homonuclear dipolar coupled nuclei under both static and MAS conditions. In most cases, this results from a reduction in dipolar dephasing and concomitant increases in $T_2^{eff}$'s in comparison to conventional approaches for acquiring SSNMR spectra of such systems. When weak homonuclear dipolar coupling exists, small θ pulses attenuate the dipolar dephasing while also partially refocusing the dominant anisotropic interaction (where θ varies for dominant linear or bilinear interactions, *vide supra*). A balance needs to be struck between maximizing the measured $T_2^{eff}$ by using a small θ to reduce dipolar dephasing, while also minimizing losses of sub-optimal small-θ refocusing of the dominant anisotropic interaction. This has been demonstrated with $^{13}C$ NMR, $^{2}H$-labelled samples having $^{2}H$-$^{2}H$ dipolar coupling constants of varying numbers and magnitudes, several $I = 3/2$ nuclei that experience various homonuclear dipolar coupling conditions, and numerical simulations on isolated spin pairs. Depending on the coupling conditions signal is enhanced by a factor as large as 3.2. The manifestation of this effect is strongest under static conditions, but is attenuated under MAS conditions, since the secular manifestation of the dipolar tensor is largely averaged in the latter case. However, under certain circumstances, $R^2$ recoupling can occur and partially reintroduce the homonuclear dipolar coupling under MAS, potentially allowing for $T_2^{eff}$ enhancement by shorter refocusing pulses if effective dipolar couplings are strong enough. It is anticipated this effect may occur for systems that have common isotopes such as $^{2}H$, $^{13}C$, $^{15}N$, and $^{17}O$, but the degree to which it manifests will be strongly dependent on the degree of isotopic enrichment. This effect should also be observed for high-γ and high n.a. nuclei such as $^{11}B$, $^{19}F$, $^{27}Al$, $^{31}P$, *etc*. in most cases. It may be

possible to use measured $T_2^{eff}$'s from variable refocusing flip angles and the dipolar oscillations in CPMG echo trains to establish internuclear distances in some cases. We anticipate that such modified CPMG pulse sequences that suppress weak homonuclear dipolar coupling can be readily applied to a multitude of NMR-active nuclei from across the periodic table, providing unique insights into structure and bonding.

## 5. Supplementary Material

See supplementary material for additional simulations, experiments, and experimental details.

## 6. Acknowledgments

R.W.S. and A.R.A would like to thank the National Science Foundation Chemical Measurement and Imaging Program, with partial co-funding from the Solid State and Materials Chemistry Program (NSF-2003854), for supporting this work. The National High Magnetic Field Laboratory is supported by the National Science Foundation through NSF/DMR-1644779 and the State of Florida. Adrian Gonzalez-Nelson is thanked for synthesising MIL-53(Al)-$d_4$ and Austin Peach is thanked for synthesizing benzoic acid-*d* and dimedone-*d*.

## 7. Data Availability

All simulation input files, pulse programs, and NMR datasets are available from the authors upon request.



Journal Pre-proofs

## 8. References


(1) Carr, H. Y.; Purcell, E. M. *Phys. Rev.* **1954**, *94*, 630–638.

(2) Meiboom, S.; Gill, D. *Rev. Sci. Instrum.* **1958**, *29*, 688–691.

(3) Shore, S. E.; Ansermet, J.; Slichter, C. P.; Sinfelt, J. H. *Phys. Rev. Lett.* **1987**, *58*, 953–956.

(4) Barrett, S. E.; Durand, D. J.; Pennington, C. H.; Slichter, C. P.; Friedmann, T. A.; Rice, J. P.; Ginsberg, D. M. *Phys. Rev. B* **1990**, *41*, 6283–6296.

(5) De Soto, S. M.; Slichter, C. P.; Kini, A. M.; Wang, H. H.; Geiser, U.; Williams, J. M. *Phys. Rev. B* **1995**, *52*, 10364–10368.

(6) Bloom, M.; Sternin, E. *Biochemistry* **1987**, *26*, 2101–2105.

(7) Larsen, F. H.; Jakobsen, H. J.; Ellis, P. D.; Nielsen, N. C. *Chem. Phys. Lett.* **1998**, *292*, 467–473.

(8) Larsen, F. H. *Solid State Nucl. Magn. Reson.* **2007**, *31*, 100–114.

(9) Larsen, F. H. *Simulation of Molecular Motion of Quadrupolar Nuclei in Solid-State NMR Spectra*. In *Annual Reports on NMR Spectroscopy*; Elsevier Ltd, 2010; Vol. 71, pp 103–137.

(10) Hung, I.; Gan, Z. *J. Magn. Reson.* **2010**, *204*, 256–265.

(11) Iijima, T.; Nishimura, K. *Chem. Phys. Lett.* **2011**, *514*, 181–186.

(12) Iijima, T.; Shimizu, T.; Nishimura, K. *J. Magn. Reson.* **2015**, *251*, 57–64.

(13) O'Dell, L. A.; Schurko, R. W. *Chem. Phys. Lett.* **2008**, *464*, 97–102.




Journal Pre-proofs

(14) Schurko, R. W. *Acquisition of Wideline Solid-State NMR Spectra of Quadrupolar Nuclei*. In *Encyclopedia of Magnetic Resonance*; John Wiley & Sons, Ltd: Chichester, UK, 2011; pp 77–93.

(15) Schurko, R. W. *Acc. Chem. Res.* **2013**, *46*, 1985–1995.

(16) O'Dell, L. A.; Rossini, A. J.; Schurko, R. W. *Chem. Phys. Lett.* **2009**, *468*, 330–335.

(17) Jardón-Álvarez, D.; Bovee, M. O.; Baltisberger, J. H.; Grandinetti, P. J. *Phys. Rev. B* **2019**, *100*, 140103.

(18) Jardón-álvarez, D.; Bovee, M. O.; Grandinetti, P. J. *J. Magn. Reson.* **2021**, 107097.

(19) Bennett, A. E.; Rienstra, C. M.; Auger, M.; Lakshmi, K. V.; Griffin, R. G. *J. Chem. Phys.* **1995**, *103*, 6951–6958.

(20) Hodgkinson, P. *Prog. Nucl. Magn. Reson. Spectrosc.* **2005**, *46*, 197–222.

(21) Siegel, R.; Nakashima, T. T.; Wasylishen, R. E. *J. Phys. Chem. B* **2004**, *108*, 2218–2226.

(22) Veinberg, S. L.; Friedl, Z. W.; Harris, K. J.; O'Dell, L. A.; Schurko, R. W. *CrystEngComm* **2015**, *17*, 5225–5236.

(23) Veinberg, S. L.; Friedl, Z. W.; Lindquist, A. W.; Kispal, B.; Harris, K. J.; O'Dell, L. A.; Schurko, R. W. *ChemPhysChem* **2016**, *17*, 4011–4027.

(24) Waugh, J. S.; Huber, L. M.; Haeberlen, U. *Phys. Rev. Lett.* **1968**, *20*, 180–182.

(25) Goldburg, W. I.; Lee, M. *Phys. Rev. Lett.* **1963**, *11*, 255–258.

(26) Sakellariou, D.; Lesage, A.; Hodgkinson, P.; Emsley, L. *Chem. Phys. Lett.* **2000**, *319*, 253–260.

(27) Paruzzo, F. M.; Emsley, L. *J. Magn. Reson.* **2019**, *309*, 106598.

(28) Ostroff, E. D.; Waugh, J. S. *Phys. Rev. Lett.* **1966**, *16*, 1097–1098.

(29) Mansfield, P.; Ware, D. *Phys. Lett.* **1966**, *22*, 133–135.

(30) Waugh, J. S.; Wang, C. H.; Huber, L. M.; Vold, R. L. *J. Chem. Phys.* **1968**, *48*, 662–670.

(31) Waugh, J. S.; Wang, C. H. *Phys. Rev.* **1967**, *162*, 209–216.

(32) Rhim, W.-K.; Burum, D. P.; Elleman, D. D. *Phys. Rev. Lett.* **1976**, *37*, 1764–1766.

(33) Vega, A. J.; Vaughan, R. W. *J. Chem. Phys.* **1978**, *68*, 1958–1966.

(34) Suwelack, D.; Waugh, J. S. *Phys. Rev. B* **1980**, *22*, 5110–5114.

(35) Siegel, R.; Nakashima, T. T.; Wasylishen, R. E. *Concepts Magn. Reson. Part A* **2005**, *26A*, 62–77.

(36) Andrew, E. R.; Bradbury, A.; Eades, R. G.; Wynn, V. T. *Phys. Lett.* **1963**, *4*, 99–100.

(37) Kubo, A.; McDowell, C. A. *J. Chem. Soc. Faraday Trans. 1 Phys. Chem. Condens. Phases* **1988**, *84*, 3713.

(38) Colombo, M. G.; Meier, B. H.; Ernst, R. R. *Chem. Phys. Lett.* **1988**, *146*, 189–196.

(39) Smith, S. O. *Encycl. Magn. Reson.* **2007**, 4–8.

(40) Edén, M. *Solid State Nucl. Magn. Reson.* **2009**, *36*, 1–10.

(41) Raleigh, D. P.; Levitt, M. H.; Griffin, R. G. *Chem. Phys. Lett.* **1988**, *146*, 71–76.

(42) Gan, Z.-H.; Grant, D. M. *Mol. Phys.* **1989**, *67*, 1419–1430.

(43) Gan, Z.; Robyr, P. *Mol. Phys.* **1998**, *95*, 1143–1152.



Journal Pre-proofs

(44) Kwak, H.-T.; Srinivasan, P.; Quine, J.; Massiot, D.; Gan, Z. *Chem. Phys. Lett.* **2003**, *376*, 75–82.

(45) Iuga, D.; Morais, C.; Gan, Z.; Neuville, D. R.; Cormier, L.; Massiot, D. *J. Am. Chem. Soc.* **2005**, *127*, 11540–11541.

(46) Edén, M.; Frydman, L. *J. Phys. Chem. B* **2003**, *107*, 14598–14611.

(47) Khudozhitkov, A. E.; Jobic, H.; Freude, D.; Haase, J.; Kolokolov, D. I.; Stepanov, A. G. *J. Phys. Chem. C* **2016**, *120*, 21704–21709.

(48) Altenhof, A. R.; Lindquist, A. W.; Foster, L. D. D.; Holmes, S. T.; Schurko, R. W. *J. Magn. Reson.* **2019**, *309*, 106612.

(49) Gonzalez-Nelson, A.; Mula, S.; Šimėnas, M.; Balčiūnas, S.; Altenhof, A. R.; Vojvodin, C. S.; Canossa, S.; Banys, J.; Schurko, R. W.; Coudert, F.-X.; et al. *J. Am. Chem. Soc.* **2021**, *143*, 12053–12062.

(50) Gan, Z.-H.; Grant, D. M. *Chem. Phys. Lett.* **1990**, *168*, 304–308.

(51) Gan, Z.; Grant, D. M.; Ernst, R. R. *Chem. Phys. Lett.* **1996**, *254*, 349–357.

(52) Bak, M.; Rasmussen, J. T.; Nielsen, N. C. *J. Magn. Reson.* **2011**, *213*, 366–400.

(53) Edén, M. *Concepts Magn. Reson. Part A Bridg. Educ. Res.* **2003**, *18*, 24–55.

(54) Fenzke, D.; Freude, D.; Fröhlich, T.; Haase, J. *Chem. Phys. Lett.* **1984**, *111*, 171–175.

(55) Kentgens, A. P. M. *Geoderma* **1997**, *80*, 271–306.

(56) Hürlimann, M. .; Griffin, D. . *J. Magn. Reson.* **2000**, *143*, 120–135.

(57) Hürlimann, M. D. *J. Magn. Reson.* **2007**, *184*, 114–129.



Journal Pre-proofs

(58) Altenhof, A. R.; Jaroszewicz, M. J.; Lindquist, A. W.; Foster, L. D. D.; Veinberg, S. L.; Schurko, R. W. *J. Phys. Chem. C* **2020**, *124*, 14730–14744.

(59) Mansfield, P. *Phys. Rev.* **1965**, *137*, A961–A974.

(60) Haeberlen, U.; Waugh, J. S. *Phys. Rev.* **1968**, *175*, 453–467.

(61) Schmidt-Rohr, K.; Saalwächter, K.; Liu, S.-F.; Hong, M. *J. Am. Chem. Soc.* **2001**, *123*, 7168–7169.

(62) Chen, H. Y.; Tycko, R. *J. Magn. Reson.* **2020**, *313*, 106715.

(63) Mehring, M. *Principles of High Resolution NMR in Solids*; Springer Berlin Heidelberg: Berlin, Heidelberg, 1983.

(64) Levitt, M. H. *Spin Dynamics*; John Wiley & Sons Ltd, 2008.

(65) Aue, W. P.; Karhan, J.; Ernst, R. R. *J. Chem. Phys.* **1976**, *64*, 4226–4227.

(66) Segawa, T. F.; Bodenhausen, G. *eMagRes* **2013**, *2*, 245–251.

(67) Gullion, T.; Pennington, C. H. *Chem. Phys. Lett.* **1998**, *290*, 88–93.

(68) Nagayama, K.; Wüthrich, K.; Ernst, R. R. *Biochem. Biophys. Res. Commun.* **1979**, *90*, 305–311.

(69) Griesinger, C.; Sørensen, O. W.; Ernst, R. R. *J. Am. Chem. Soc.* **1985**, *107*, 6394–6396.

(70) Griesinger, C.; Sørensen, O. .; Ernst, R. . *J. Magn. Reson.* **1987**, *75*, 474–492.

(71) Schulte-Herbrüggen, T.; Mádi, Z. L.; Sørensen, O. W.; Ernst, R. R. *Mol. Phys.* **1991**, *72*, 847–871.



Journal Pre-proofs

(72) Orendt, A. M.; Facelli, J. C.; Radziszewski, J. G.; Horton, W. J.; Grant, D. M.; Michl, J. *J. Am. Chem. Soc.* **1996**, *118*, 846–852.

(73) Xue, X. *Solid State Nucl. Magn. Reson.* **2010**, *38*, 62–73.

(74) Maricq, M.; Waugh, J. S. *Chem. Phys. Lett.* **1977**, *47*, 327–329.

(75) Herzfeld, J.; Berger, A. E. *J. Chem. Phys.* **1980**, *73*, 6021–6030.

(76) Samoson, A.; Tuherm, T.; Gan, Z. *Solid State Nucl. Magn. Reson.* **2001**, *20*, 130–136.

(77) Chávez, M.; Wiegand, T.; Malär, A. A.; Meier, B. H.; Ernst, M. *Magn. Reson.* **2021**, *2*, 499–509.

(78) Simões de Almeida, B.; Moutzouri, P.; Stevanato, G.; Emsley, L. *J. Chem. Phys.* **2021**, *155*, 084201.

(79) Cowans, B. A.; Grutzner, J. B. *J. Magn. Reson. Ser. A* **1993**, *105*, 10–18.

(80) Dementyev, A. E.; Li, D.; MacLean, K.; Barrett, S. E. *Phys. Rev. B* **2003**, *68*, 153302.

(81) Li, D.; Dementyev, A. E.; Dong, Y.; Ramos, R. G.; Barrett, S. E. *Phys. Rev. Lett.* **2007**, *98*, 190401.

(82) Li, D.; Dong, Y.; Ramos, R. G.; Murray, J. D.; MacLean, K.; Dementyev, A. E.; Barrett, S. E. *Phys. Rev. B - Condens. Matter Mater. Phys.* **2008**, *77*, 1–26.

(83) Antonijevic, S.; Wimperis, S. *J. Magn. Reson.* **2003**, *164*, 343–350.

(84) Iijima, T.; Shimizu, T. *Solid State Nucl. Magn. Reson.* **2018**, *91*, 1–8.

(85) Müller, C.; Schajor, W.; Zimmermann, H.; Haeberlen, U. *J. Magn. Reson.* **1984**, *56*, 235–246.



Journal Pre-proofs

(86) Aliev, A. E.; Mann, S. E.; Rahman, A. S.; McMillan, P. F.; Corà, F.; Iuga, D.; Hughes, C. E.; Harris, K. D. M. M.; Cora, F.; Iuga, D.; et al. *J. Phys. Chem. A* **2011**, *115*, 12201–12211.

(87) Ziener, C. H.; Kampf, T.; Jakob, P. M.; Bauer, W. R. *J. Magn. Reson.* **2010**, *202*, 38–42.

(88) Gan, Z.; Robyr, P.; Ernst, R. R. *Chem. Phys. Lett.* **1998**, *283*, 262–268.

(89) Stöckli, A.; Meier, B. H.; Kreis, R.; Meyer, R.; Ernst, R. R. *J. Chem. Phys.* **1990**, *93*, 1502–1520.

(90) Wu, G.; Hung, I.; Gan, Z.; Terskikh, V.; Kong, X. *J. Phys. Chem. A* **2019**, *123*, 8243–8253.

(91) Wi, S.; Frydman, L. *J. Chem. Phys.* **2000**, *112*, 3248–3261.

(92) Shamsuzzoha, M.; Lucas, B. W. *Acta Crystallogr. Sect. B Struct. Crystallogr. Cryst. Chem.* **1982**, *38*, 2353–2357.

(93) Massiot, D.; Touzo, B.; Trumeau, D.; Coutures, J. P.; Virlet, J.; Florian, P.; Grandinetti, P. J. *Solid State Nucl. Magn. Reson.* **1996**, *6*, 73–83.

(94) Iuga, D.; Holland, D.; Dupree, R. *J. Magn. Reson.* **2014**, *246*, 122–129.

(95) Wolf, T.; Jaroszewicz, M. J.; Frydman, L. *J. Phys. Chem. C* **2020**.

(96) Gee, B.; Eckert, H. *Solid State Nucl. Magn. Reson.* **1995**, *5*, 113–122.

(97) Duer, M. J. *Chem. Phys. Lett.* **1997**, *277*, 167–174.

(98) Duer, M. J.; Painter, A. J. *Chem. Phys. Lett.* **1999**, *313*, 763–770.

(99) Fuess, H.; Hohlwein, D.; Mason, S. A. *Acta Crystallogr. Sect. B Struct. Crystallogr.*



Journal Pre-proofs

*Cryst. Chem.* **1977**, *33*, 654–659.

(100) Vega, A. J. *Quadrupolar Nuclei in Solids*. In *Solid State NMR Studies of Biopolymers*; John Wiley & Sons Ltd: Chichester, U.K., 2010.

(101) Schreyer, M.; Guo, L.; Thirunahari, S.; Gao, F.; Garland, M. *J. Appl. Crystallogr.* **2014**, *47*, 659–667.

(102) Zavodnik, V.; Stash, A.; Tsirelson, V.; de Vries, R.; Feil, D. *Acta Crystallogr. Sect. B Struct. Sci.* **1999**, *55*, 45–54.

(103) Wilson, C. C.; Nowell, H. *New J. Chem.* **2000**, *24*, 1063–1066.

(104) Wilson, C. C.; Shankland, N.; Florence, A. J. *J. Chem. Soc. Faraday Trans.* **1996**, *92*, 5051.

(105) Ortiz, G.; Chaplais, G.; Paillaud, J.-L.; Nouali, H.; Patarin, J.; Raya, J.; Marichal, C. *J. Phys. Chem. C* **2014**, *118*, 22021–22029.

(106) Bolte, M.; Scholtyssik, M. *Acta Crystallogr. Sect. C Cryst. Struct. Commun.* **1997**, *53*, IUC9700013.

(107) Tanaka, K.; Naruse, H.; Morikawa, H.; Marumo, F. *Acta Crystallogr. Sect. B Struct. Sci.* **1991**, *47*, 581–588.

Journal Pre-proofs

## Tables

**Table I**: Homonuclear dipolar coupling constants, measured $T_2^{eff}$'s, and signal enhancements for $^2$H-labelled samples in this work.

| Sample | Shortest $r_D$ (Å)† | $\nu_D$ (Hz) | $T_2^{eff,90}$ (ms) | $T_2^{eff,45}$ (ms) | $S_{45}/S_{90}$‡ | Reference |
|---|---|---|---|---|---|---|
| α-glycine-$d_2$ | 1.817 | 472 | 3.19 | 11.96 | 1.90 | [101] |
| Urea-$d_4$ | 1.739 | 538 | 1.09 | 3.33 | 1.33 | [102] |
| DMNAP-$d_{12}$ | 2.124 | 295 | 2.64 | 8.36, 12.13* | 1.49, 1.69* | [103] |
| Benzoic acid-$d$ | 2.262 | 245 | 48.8 | 74.22 | 0.81 | [104] |
| MIL-53-$d_4$ | 2.387 | 208 | 8.224 | 23.11 | 1.08 | [105] |
| Dimedone-$d$ | 5.030 | 22.2 | 22.14 | 31.33 | 0.84 | [106] |

† For samples that have multiple homonuclear dipolar couplings, the spin pair with the shortest average internuclear distance is reported, along with the corresponding dipolar coupling constant, $\nu_D$.
‡ The ratio of the integrated signal intensity of the powder patterns acquired with 45° and 90° refocusing pulses.
* Results using $\tau_{ref}$ = 1.0 μs (36°), which yielded the largest enhancements only in the case of DMNAP-$d_{12}$.

Journal Pre-proofs

**Table II**: Homonuclear dipolar coupling constants of half-integer spin quadrupolar nuclei in samples in this work, measured $T_2^{eff}$'s, and signal enhancements.

| **Sample (Nucleus)** | **Shortest $r_D$ (Å)†** | **$\nu_D$ (Hz)** | **$\nu_{rot}$ (kHz)** | **$T_2^{eff,180}$ (ms)** | **$T_2^{eff,\theta}$ (ms)*** | **$S_\theta/S_{90}$‡** | **θ** | **Reference** |
|---|---|---|---|---|---|---|---|---|
| $RbNO_3$ ($^{87}Rb$) | 3.85 | 227 | 0 | 2.6 | 12.9 | 2.61 | 90 | [92] |
| | | | 10 | 62.6 | 82.6 | 0.77 | 90 | |
| $Na_2SO_4$ ($^{23}Na$) | 3.25 | 245 | 0 | 0.60 | 1.63 | 2.95 | 72 | [107] |
| | | | 10 | 8.15 | 22.47 | 2.44 | 90 | |
| L-Histidine HCl□$H_2O$ ($^{35}Cl$) | 5.775 | 6 | 0 | 31.7 | 41.5 | 1.03 | 144 | [99] |

† For samples that have multiple homonuclear dipolar couplings, the spin pair with the shortest average internuclear distance is reported, along with the corresponding dipolar coupling constant, $\nu_D$.

* The $T_2^{eff}$ is measured when using a refocusing pulse of flip angle θ that varies between systems and experiments and is detailed in the text and the corresponding figures.

‡ The ratio of the integrated signal intensity of the powder pattern acquired with θ and 90° refocusing pulses.

Journal Pre-proofs

**Figure Captions**

**Figure 1**. Experimental $^{1}H$-$^{13}C$ CP-CPMG NMR FIDs (left column) and spectra (right column) of 1,2-phthalic anhydride-$^{13}C_2$ acquired under static conditions using a RF amplitude of 100 kHz for all pulses, an excitation pulse width ($\tau_{exc}$) of 2.5 μs, and a refocusing pulse width ($\tau_{ref}$) that is varied between 5 μs – 1.25 μs (a – e) causing the refocusing pulse flip angle (θ) to change accordingly. In every case the area of the powder pattern is displayed to the right of the pattern and is normalized with respect to the pattern in (a). The FIDs and spectra in the left and right columns, respectively, are plotted on the same relative intensity scale. The monoexponential $T_2^{eff}$'s are denoted for each FID. In every case the second echo is not fully formed (see text for details); therefore, the second echo is not included for the $T_2^{eff}$ fits.

**Figure 2**. Simulated $^{13}C$ NMR (a) powder pattern areas as a function of homonuclear dipolar couplings, $\nu_D$, and refocusing pulse widths, $\tau_{ref}$, with select FID's (middle column) and spectra (right column) of an AB spin system using CS tensor parameters of $\delta_{iso}$ = 131.67 ppm, Ω = 189.87 ppm, and κ = 0.37 for both sites, where the relative orientations of the two CS tensors is described in the main text (azimuthal angle, α = 35 °). Powder patterns are simulated with a CPMG pulse sequence using a RF amplitude of 100 kHz for all pulses, $\tau_{exc}$ = 2.5 μs, and a $\tau_{ref}$ that is varied (a) between 5 μs (180°) and 0.5 μs (18°). Select FIDs and spectra are shown for a $\tau_{ref}$ of (b) 5 μs (180°) and (c) 2.5 μs (90°) without a homonuclear dipolar coupling and (d, e) the same refocusing pulses, respectively, with $\nu_D$ = 2790 Hz. Blue lines show which set of FIDs and spectra correspond to which dipolar coupling strength in the contour plot. The areas are displayed to the right of each pattern and are normalized with respect to the pattern calculated with $\tau_{ref}$ = 5 μs (180°) in each case. All simulated echoes are coadded to calculated pattern areas.

**Figure 3**. Experimental $^{1}H$-$^{13}C$ CP/MAS NMR FIDs and spectra of 1,2-phthalic anhydride-$^{13}C_2$ acquired with spinning frequencies of (a) 10 kHz, (b) 5 kHz, and (c) 3 kHz at 18.8 T.

**Figure 4**. Experimental $^{1}H$-$^{13}C$ CP-CPMG/MAS NMR FIDs (left column) and spectra (right column) of 1,2-phthalic anhydride-$^{13}C_2$ acquired with rotor frequencies of (a, b) 5 kHz and (c, d) 3 kHz. Signal is acquired using rotor-synchronized CP-CPMG/MAS with refocusing pulse amplitudes of 100 kHz and $\tau_{ref}$ of (a, c) 5 μs (180°) and (b, d) 2.5 μs (90°). The integrated areas of the spinning sideband manifolds are displayed to the right of the patterns and normalized with respect to the area pattern acquired with $\tau_{ref}$ = 5 μs (180°). The FIDs and spectra in the left and right columns, respectively, are plotted on the same intensity scale for purposes of separately comparing (a, b) 5 kHz MAS and (c, d) 3 kHz MAS data. The monoexponential $T_2^{eff}$'s are denoted for each FID.

**Figure 5**. Experimental $^{2}$H NMR FIDs (left column) and spectra (right column) of α-glycine-$d_2$ acquired with a CPMG pulse sequence using a RF amplitude of 100 kHz for all pulses, an excitation pulse width ($\tau_{exc}$) of 2.5 μs, and a refocusing pulse width ($\tau_{ref}$) that is varied between 2.5 μs – 0.75 μs (a – h) causing the refocusing pulse flip angle (θ) to change accordingly. In every case the area of the powder pattern is displayed to the right of the pattern and is normalized with respect to the pattern in (a). The FIDs and spectra in the left and right columns, respectively, are plotted on the same relative intensity scale. The monoexponential $T_2^{eff}$'s are denoted for each FID. In every case the first three echoes are not included in the $T_2^{eff}$ fits (see text for details).

**Figure 6**. (a) Areas of numerically simulated $^{2}$H NMR powder patterns of an AB spin system as a function of homonuclear dipolar coupling strength and refocusing pulse widths and (b) - (e) select FIDs (middle column) and spectra (right column). The AB spin system has EFG tensor parameters of $C_Q$ = 159.6 kHz and 167.6 kHz and $\eta_Q$ = 0.058 and 0.084. With respect to a fixed EFG tensor for one site, the second EFG tensor is oriented at β = 109.5° and the dipolar tensor is oriented with β = 35.25°. Powder patterns are simulated with a CPMG pulse sequence using a RF amplitude of 100 kHz for all pulses, $\tau_{exc}$ = 2.5 μs, and a $\tau_{ref}$ that is varied (a) between 2.5 μs (90°) and 0.75 μs (27°). Select FIDs and spectra are shown for a $\tau_{ref}$ of (b) 2.5 μs (90°) and (c) 1.5 μs (54°) without a homonuclear dipolar coupling and (d, e) with $\nu_D$ = 450 Hz. Blue lines show which set of FIDs and spectra correspond to which dipolar coupling strength in the contour plot. The area of the powder pattern is displayed to the right and is normalized with respect to the pattern calculated with $\tau_{ref}$ = 2.5 μs (90°) in each case. All simulated echoes are coadded to calculated pattern areas.

**Figure 7**. Experimental $^{2}$H NMR FIDs (left column) and spectra (right column) of α-glycine-$d_2$ acquired under MAS with $\nu_{rot}$ = 10 kHz using a rotor-synchronized CPMG pulse sequence with RF amplitudes of 75 kHz for all pulses, $\tau_{exc}$ = 3.33 μs, and a $\tau_{ref}$ that is varied between (a) 3.33 μs (90°) and (b) 1.67 μs (45°). The areas of the spinning sideband manifolds are displayed to the right of each pattern, and are normalized with respect to the area of the pattern in (a). The FIDs and spectra in the left and right columns, respectively, are plotted on the same relative intensity scale. The monoexponential $T_2^{eff}$'s are denoted for each FID.

**Figure 8**. Experimental $^{87}$Rb NMR FIDs (left column) and spectra (right column) of $RbNO_3$ acquired with a CPMG pulse sequence using a RF amplitude of 10 kHz for all pulses, $\tau_{exc}$ = 12.5 μs, and a $\tau_{ref}$ of (a) 25 μs ($\theta_{sel}$ = 180°) and (b) 12.5 μs (90°) under static conditions and (c, d) the same refocusing pulses, respectively, under MAS conditions with $\nu_{rot}$ = 10 kHz. The area of each powder pattern is displayed to its right, and is normalized with respect to the area of the pattern acquired with $\tau_{ref}$ = 25 μs (180°) in each case. The FIDs and spectra in the left and right columns, respectively, are plotted on the same intensity scale for purposes of separately comparing (a, b) static and (c, d) MAS data. The monoexponential $T_2^{eff}$'s are denoted for each FID. In every case the first two echoes are not included in the $T_2^{eff}$ fits (see text for details).

**Figure 9**. Experimental $^{23}$Na NMR FIDs (left column) and spectra (right column) of $Na_2SO_4$ acquired with a CPMG pulse sequence using a RF amplitude of 10 kHz for all pulses, $\tau_{exc}$ = 12.5 μs, and a $\tau_{ref}$ of (a) 25 μs ($\theta_{sel}$ = 180°) and (b) 12.5 μs (90°) under static conditions and (c, d) the same refocusing pulses, respectively, under MAS conditions with $\nu_{rot}$ = 10 kHz. The area of each powder pattern is displayed to its right, and is normalized with respect to the area of the pattern acquired with $\tau_{ref}$ = 25 μs (180°) in each case. The FIDs and spectra in the left and right columns, respectively, are plotted on the same intensity scale for purposes of separately comparing (a, b) static and (c, d) MAS data. The monoexponential $T_2^{eff}$'s are denoted for each FID.

**Figure 10**. Experimental $^{35}$Cl NMR FIDs (left column) and spectra (right column) of L-histidine HCl□$H_2O$ acquired with a CPMG pulse sequence using a RF amplitude of 10 kHz for all pulses, $\tau_{exc}$ = 12.5 μs, and a $\tau_{ref}$ of (a) 25 μs ($\theta_{sel}$ = 180°) and (b) 20 μs (144°) under static conditions and (c, d) the same refocusing pulses, respectively, under MAS conditions with $\nu_{rot}$ = 10 kHz. The area of each powder pattern is displayed to its right, and is normalized with respect to the area of the pattern acquired with $\tau_{ref}$ = 25 μs (180°) in each case. The FIDs and spectra in the left and right columns, respectively, are plotted on the same intensity scale for purposes of separately comparing (a, b) static and (c, d) MAS data. The monoexponential $T_2^{eff}$'s are denoted for each FID.

**Figure 11**. Simulated $^{23}$Na NMR (a) powder pattern areas as a function of homonuclear dipolar coupling strength and refocusing pulse widths and select FID's (middle column) and spectra (right column) of an $A_2$ spin system using EFG tensor parameters of $C_Q$ = 2.6 MHz and $\eta_Q$ = 0.6 for both sites. The largest component of both EFG tensors are oriented at β = 90° with respect to the internuclear vector. Powder patterns are simulated with a CPMG pulse sequence using a RF amplitude of 10 kHz for all pulses, $\tau_{exc}$ = 12.5 μs, and $\tau_{ref}$ that is varied (a) between 50 μs ($\theta_{sel}$ = 360°) and 2.5 μs (18°). Select FIDs and spectra are shown for a $\tau_{ref}$ of (b) 25 μs (180°) and (c) 15 μs (108°) $\nu_D$ = 0 Hz and (d, e) with $\nu_D$ = 250 Hz. Blue lines show which set of FIDs and spectra correspond to which dipolar coupling strength in the contour plot. The integral of the powder pattern is displayed to the right of each pattern and is normalized with respect to the pattern calculated with $\tau_{ref}$ = 25 μs (180°) in each case. All simulated echoes are coadded to calculated pattern areas.

# Figure 1

nal Pre-pro

Journal Pre-proofs

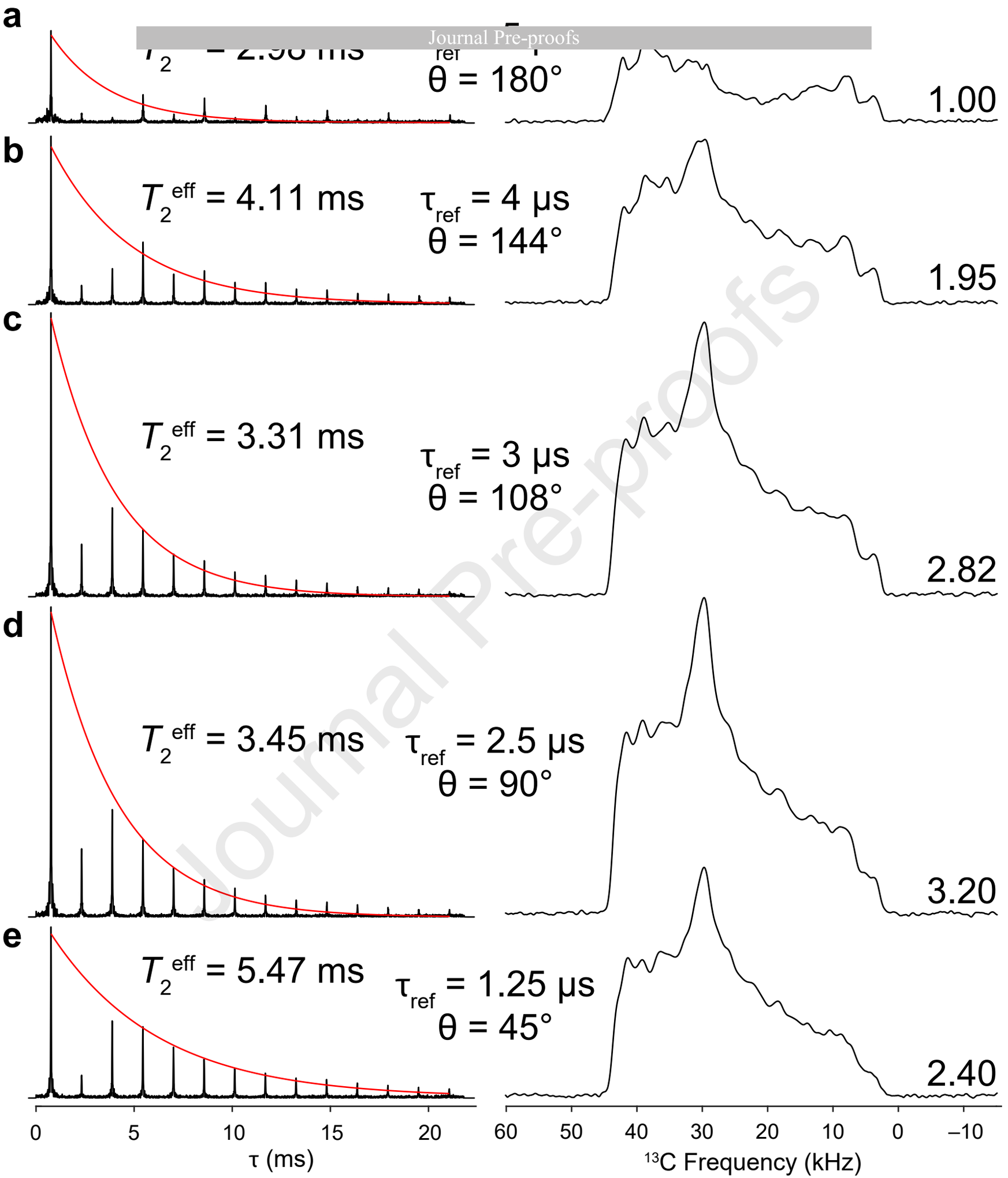


Journal Pre-proofs

# Figure 2

nal Pre-pro

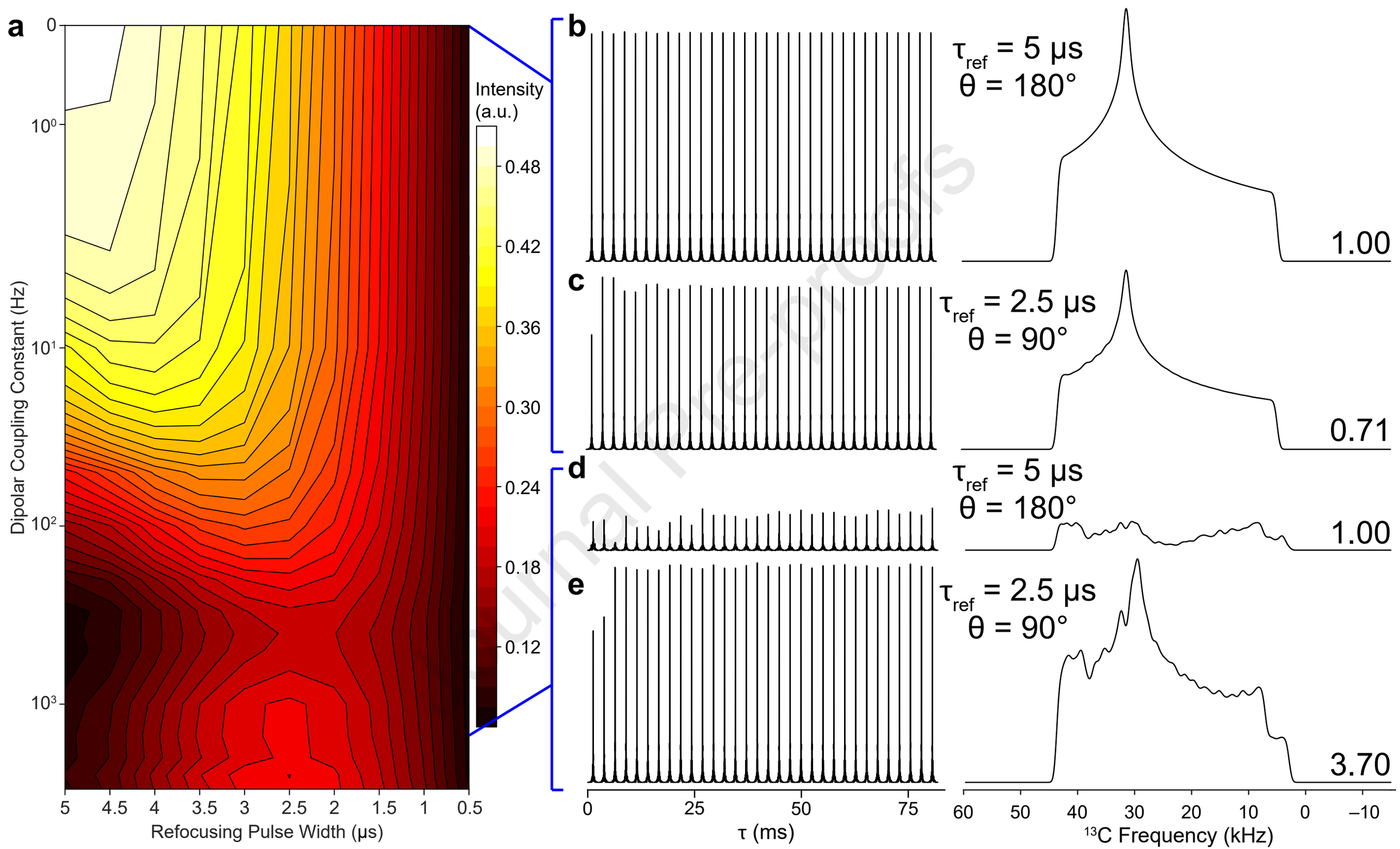
a
b
c
d
e
Intensity (a.u.)
0.48
0.42
0.36
0.30
0.24
0.18
0.12
Dipolar Coupling Constant (Hz)
0
10⁰
10¹
10²
10³
5
4.5
4
3.5
3
2.5
2
1.5
1
0.5
Refocusing Pulse Width (μs)
τref = 5 μs
θ = 180°
1.00
τref = 2.5 μs
θ = 90°
0.71
τref = 5 μs
θ = 180°
1.00
τref = 2.5 μs
θ = 90°
3.70
0
25
50
75
τ (ms)
60
50
40
30
20
10
0
–10
13C Frequency (kHz)

# Figure 3

nal Pre-pro

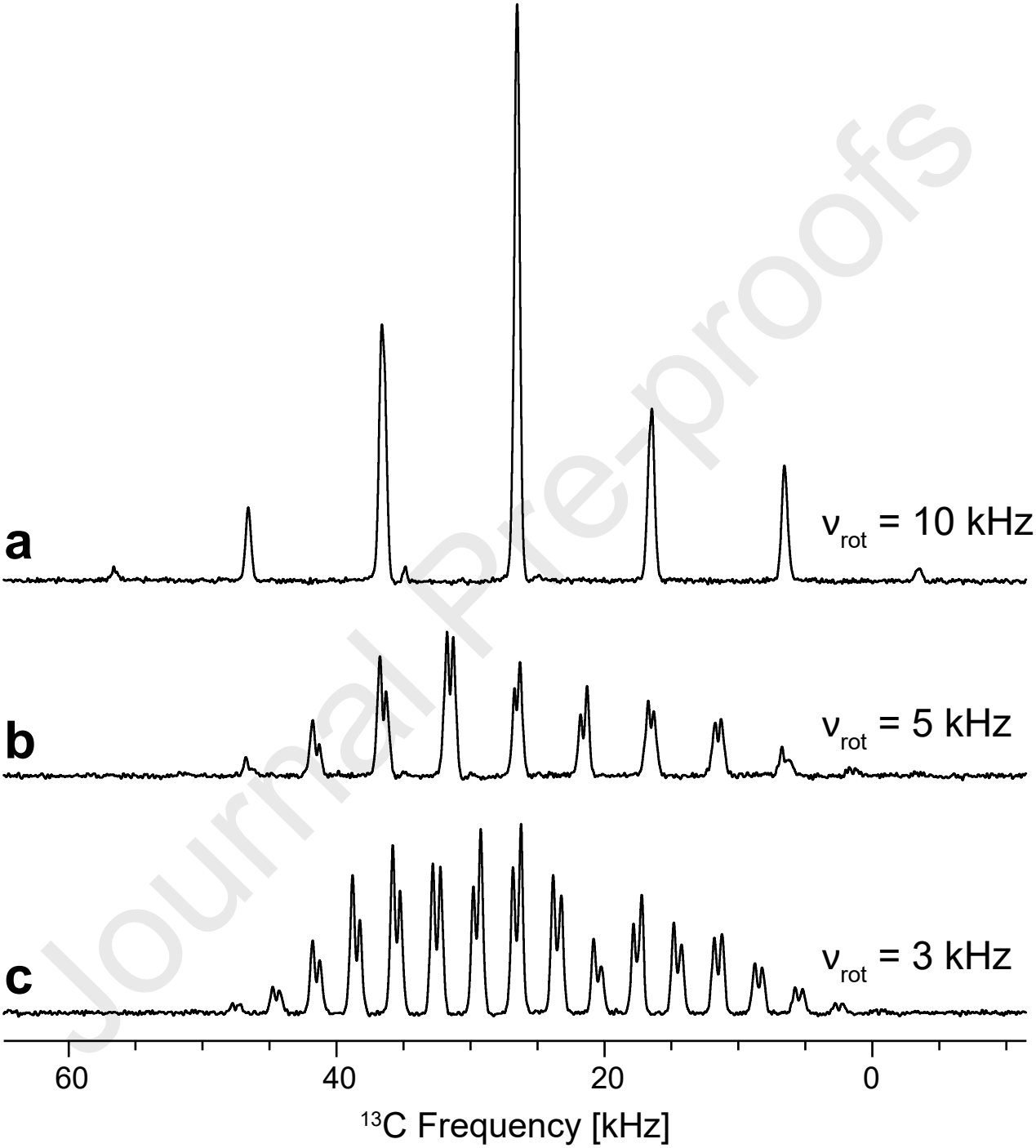


Journal Pre-proofs

# Figure 4

nal Pre-pro

Journal Pre-proofs

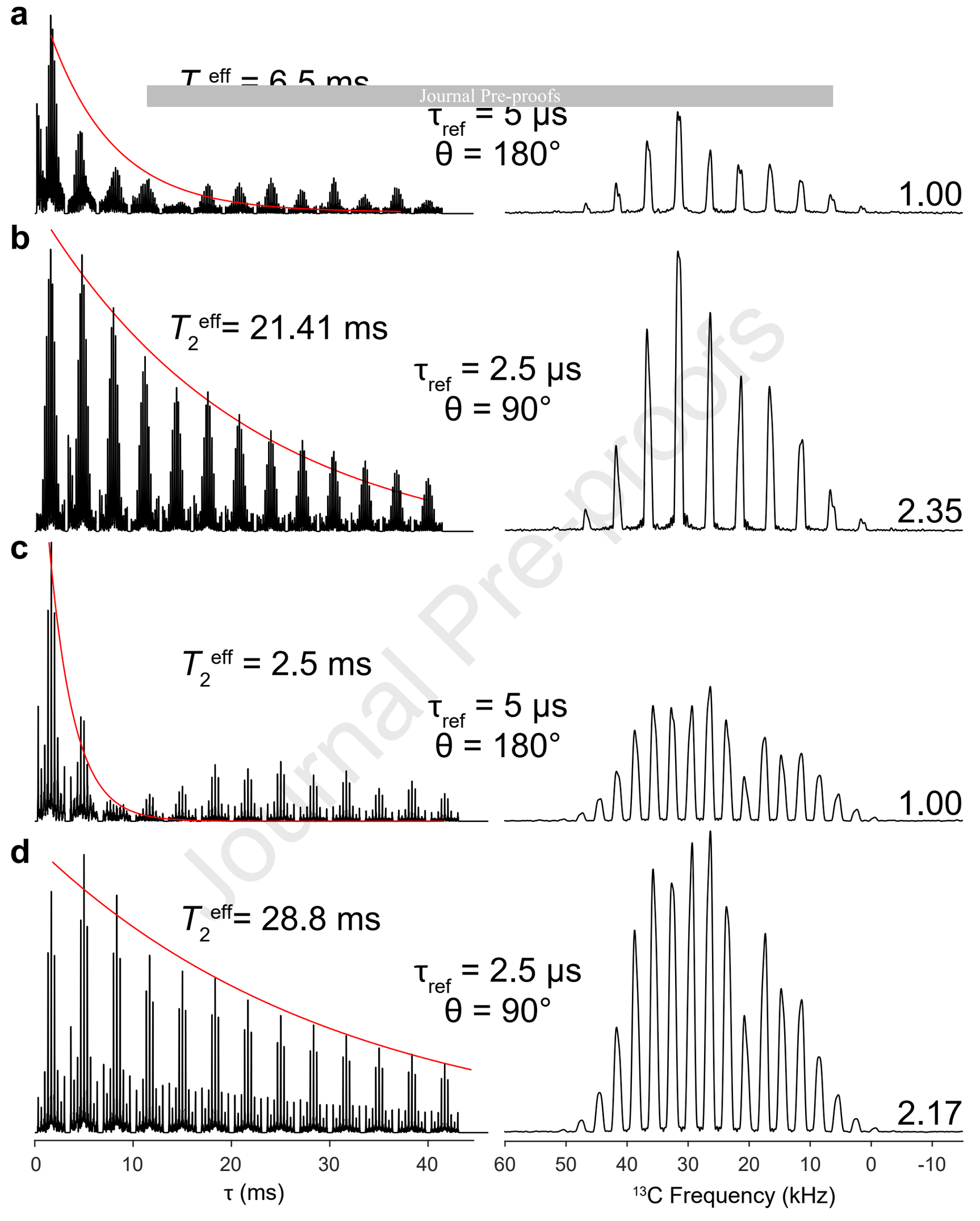


Journal Pre-proofs

# Figure 5

nal Pre-pro

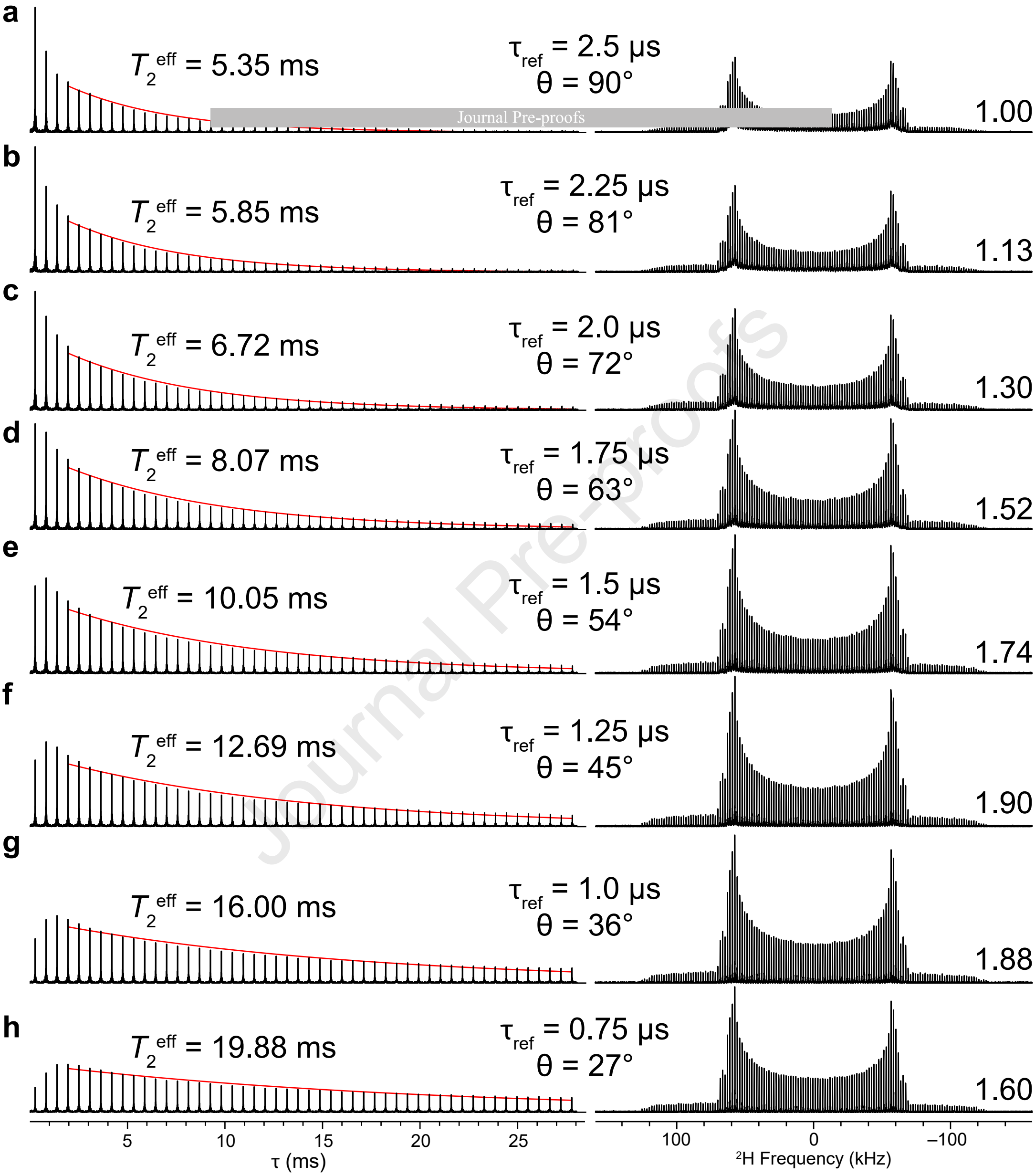


Journal Pre-proofs

# Figure 6

nal Pre-pro

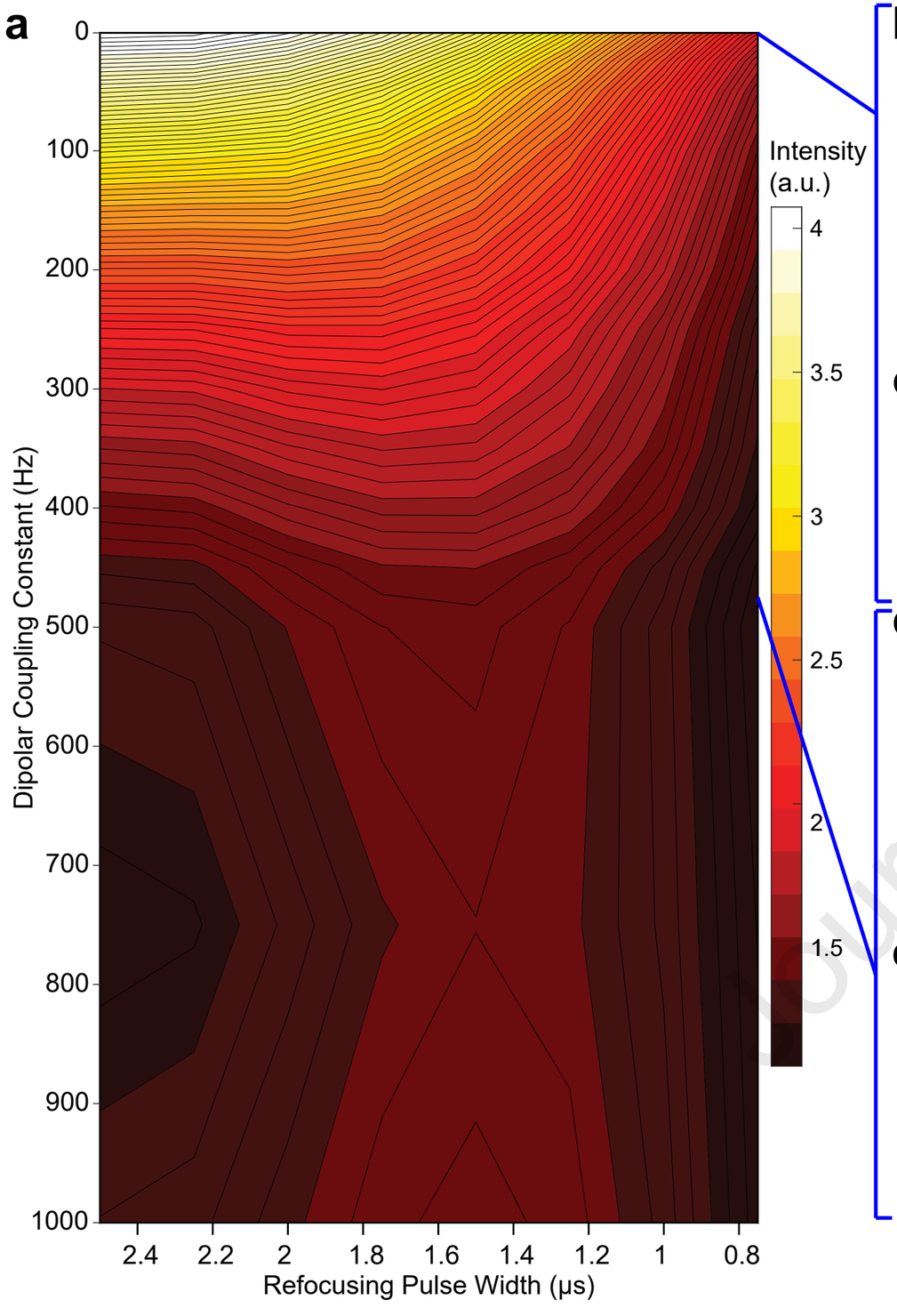


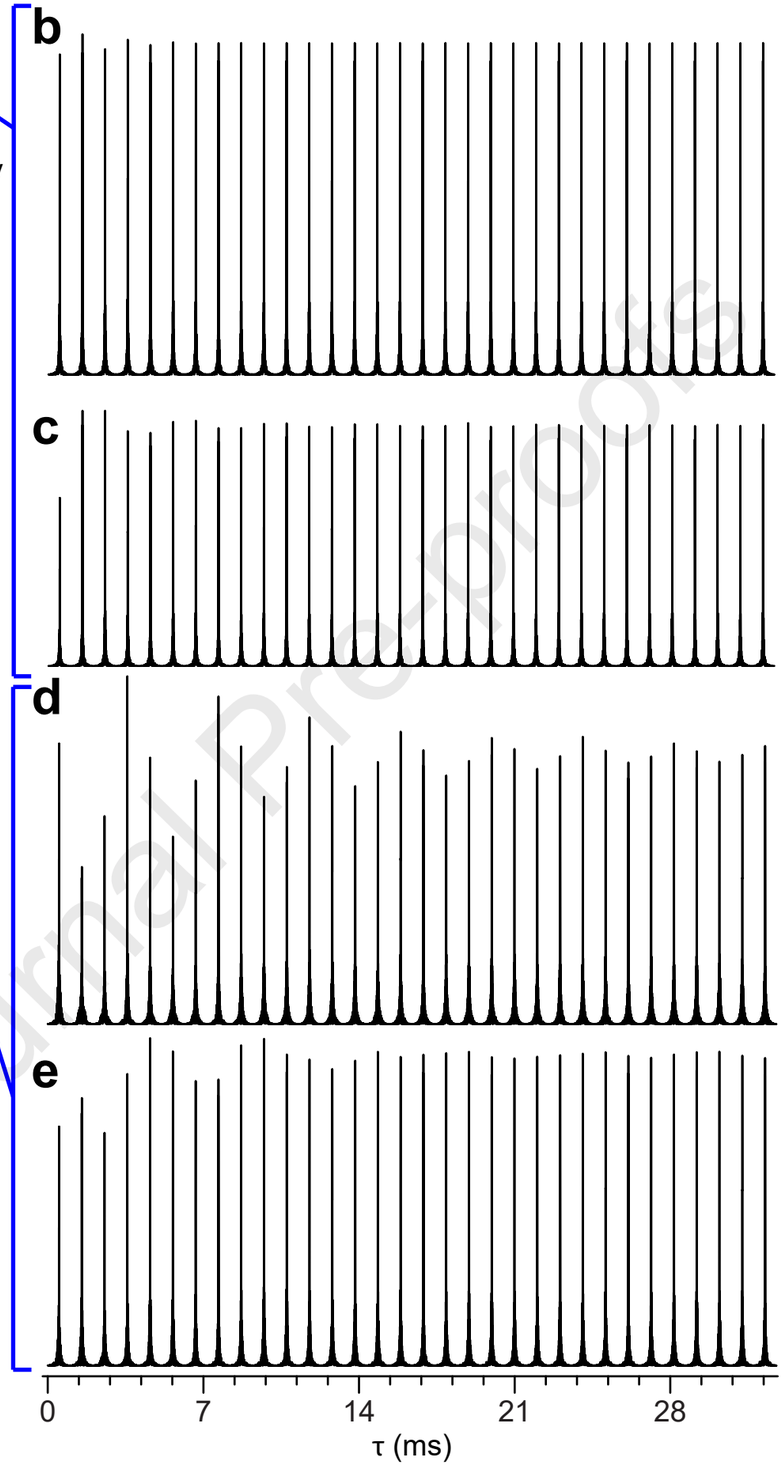


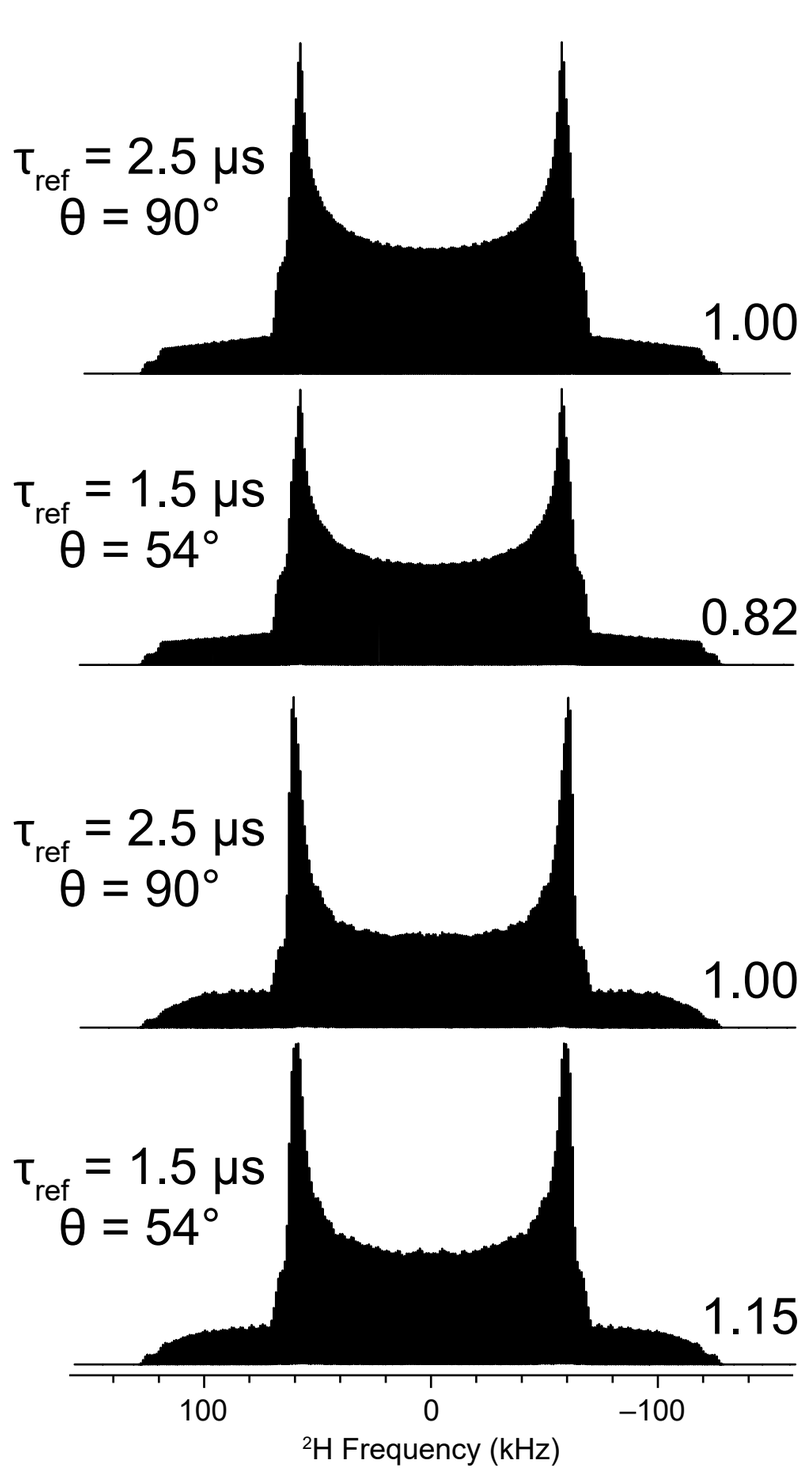


Journal Pre-proofs

# Figure 7

nal Pre-pro

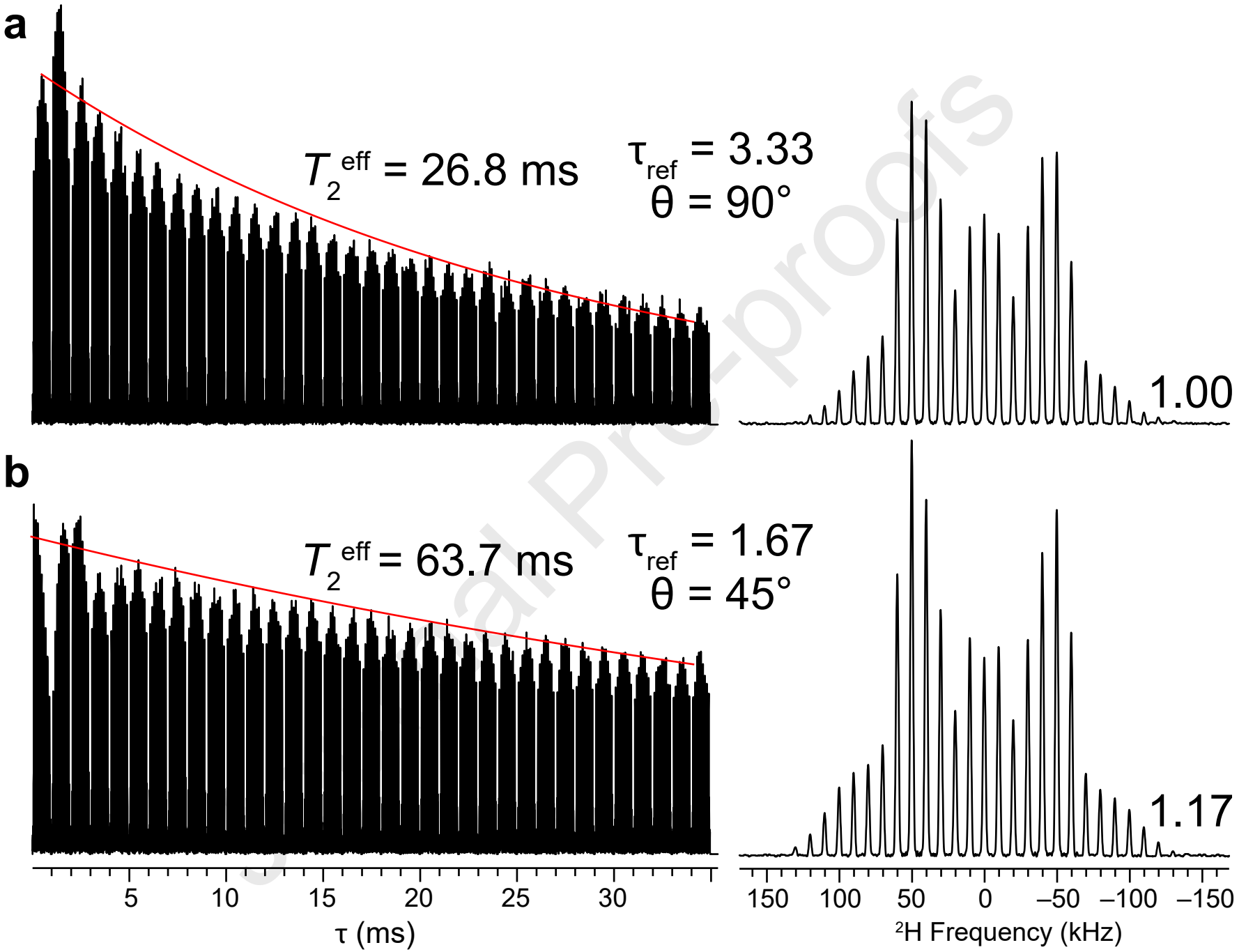


Journal Pre-proofs

# Figure 8

nal Pre-pro

Journal Pre-proofs

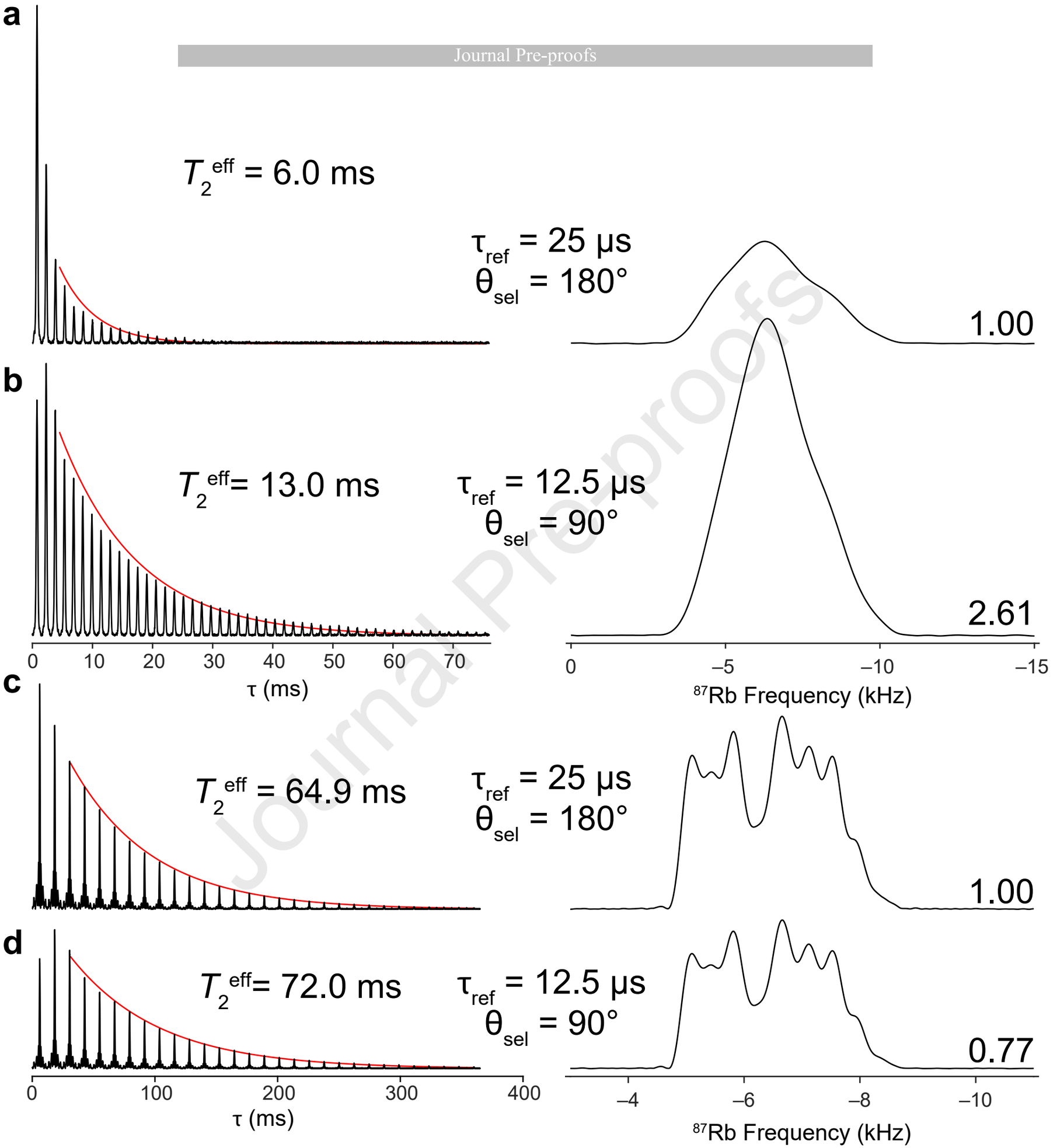


Journal Pre-proofs

# Figure 9

nal Pre-pro

Journal Pre-proofs

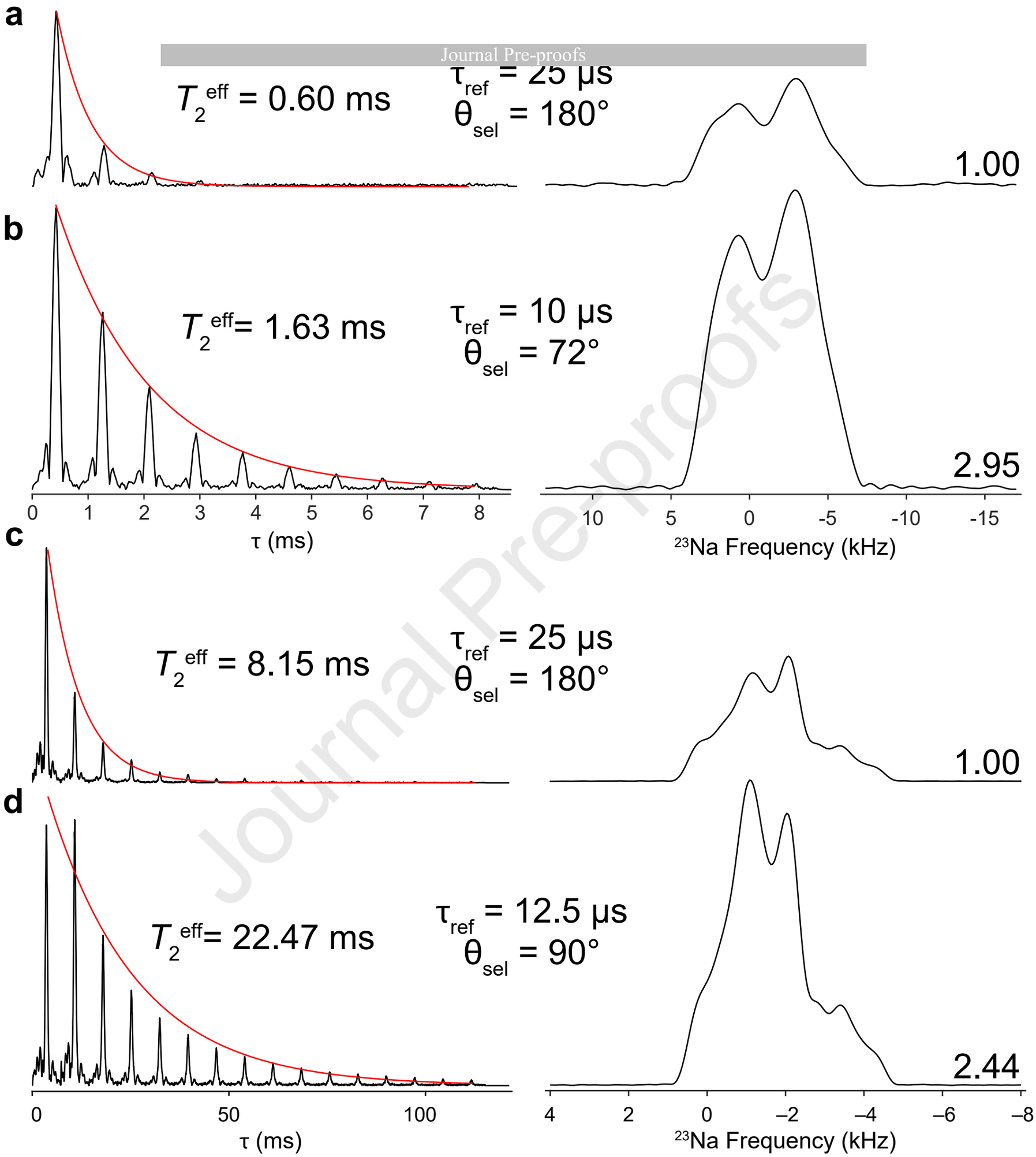


Journal Pre-proofs

# Figure 10

nal Pre-pro

Journal Pre-proofs

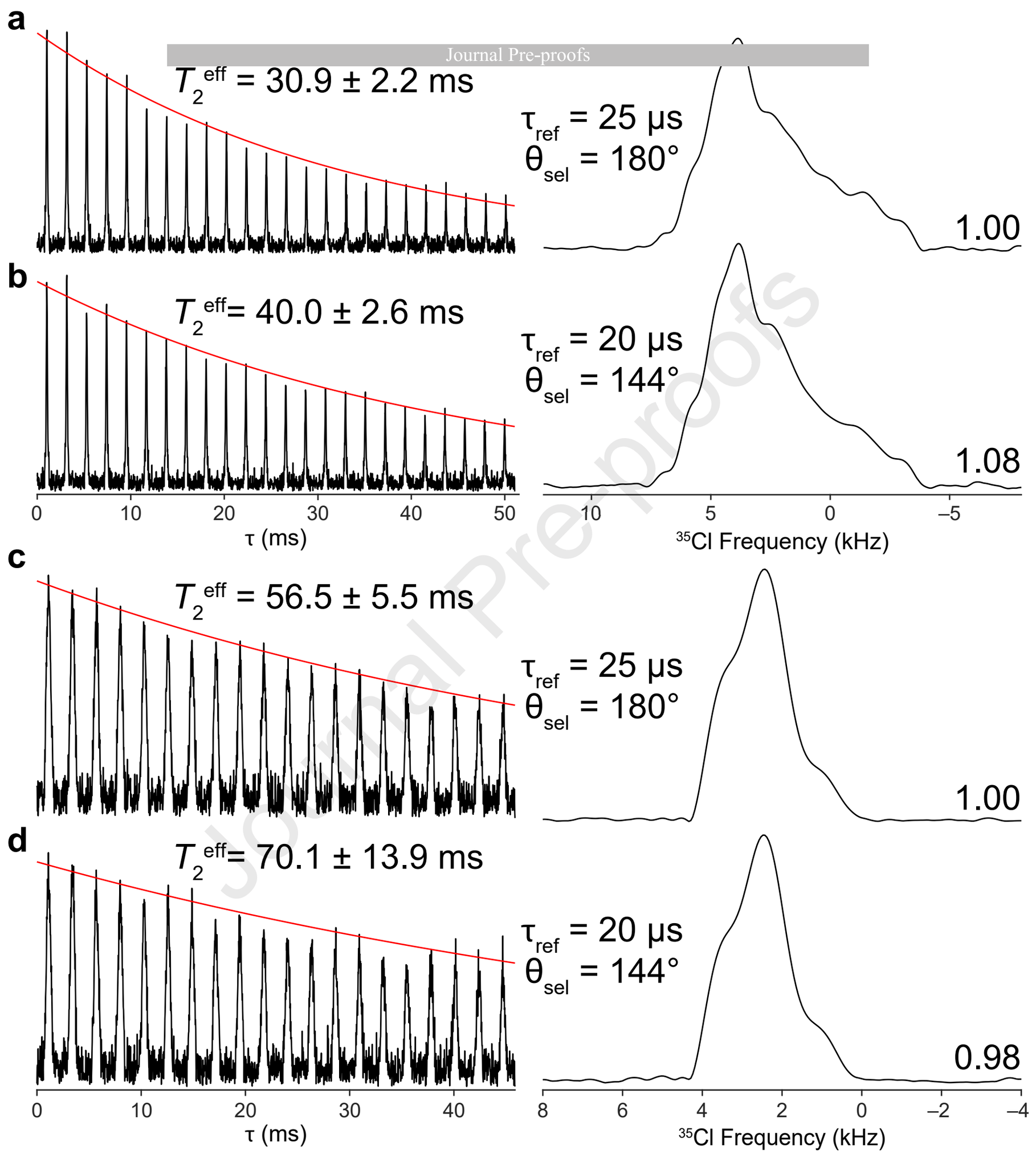


Journal Pre-proofs

# Figure 11

nal Pre-pro

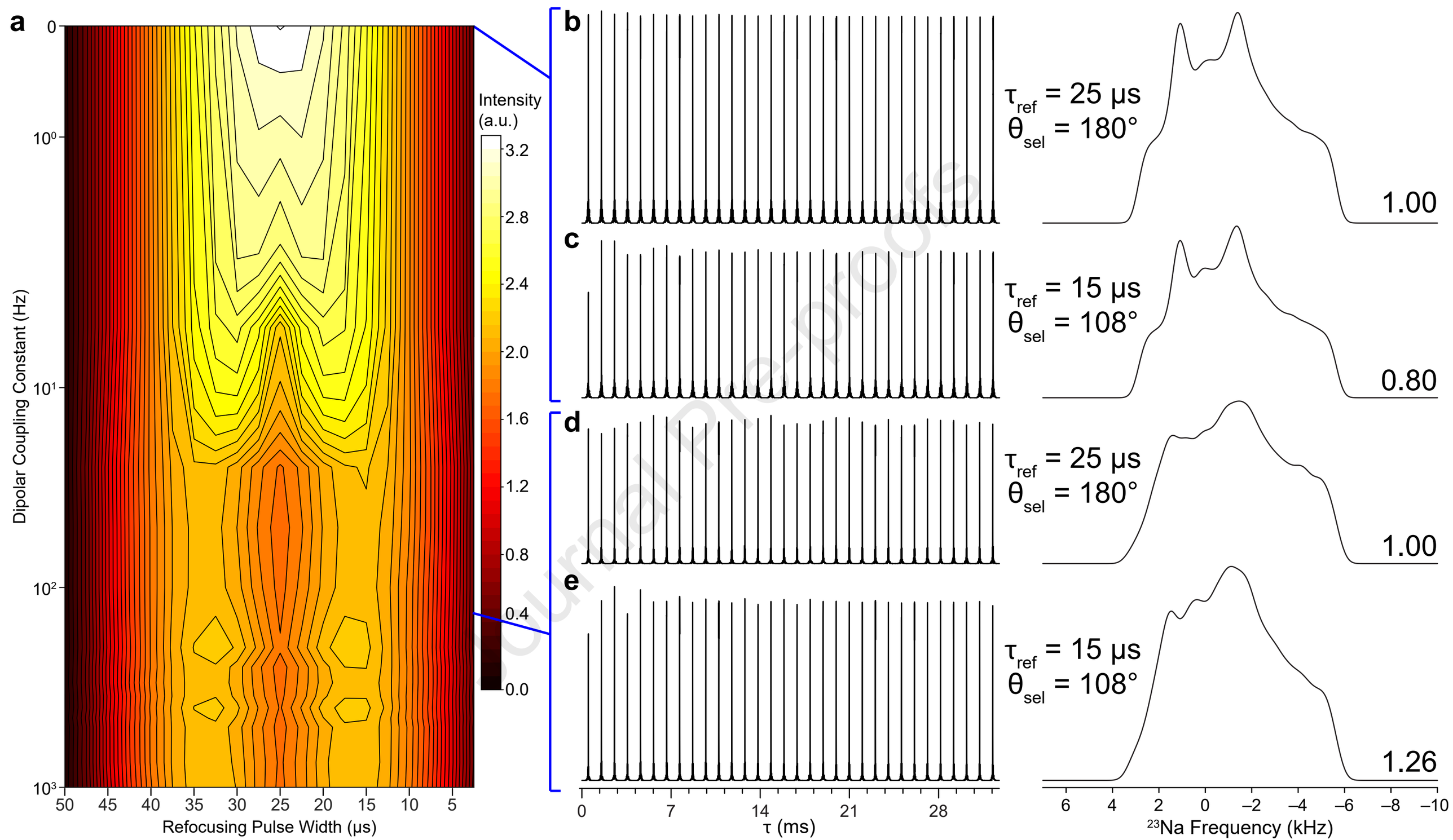
a
b
c
d
e
Intensity (a.u.)
3.2
2.8
2.4
2.0
1.6
1.2
0.8
0.4
0.0
Dipolar Coupling Constant (Hz)
$10^0$
$10^1$
$10^2$
$10^3$
50 45 40 35 30 25 20 15 10 5
Refocusing Pulse Width (μs)
$\tau_{ref}$ = 25 μs
$\theta_{sel}$ = 180°
1.00
$\tau_{ref}$ = 15 μs
$\theta_{sel}$ = 108°
0.80
$\tau_{ref}$ = 25 μs
$\theta_{sel}$ = 180°
1.00
$\tau_{ref}$ = 15 μs
$\theta_{sel}$ = 108°
1.26
0 7 14 21 28
τ (ms)
6 4 2 0 −2 −4 −6 −8 −10
$^{23}$Na Frequency (kHz)

**Highlights**

▪ Weak homonuclear dipolar interactions affect CPMG echo trains in SSNMR.
▪ Small flip angles for CPMG refocusing pulses attenuate dipolar dephasing.
▪ Measured effective coherence lifetimes (T2eff) can be extended.
▪ Significant signal enhancements can be achieved with modified CPMG pulse sequences for weak homonuclear dipolar coupled systems.
▪ These effects manifest in spectra of spin-1/2 and quadrupolar nuclei under static and MAS conditions.

Journal Pre-proofs

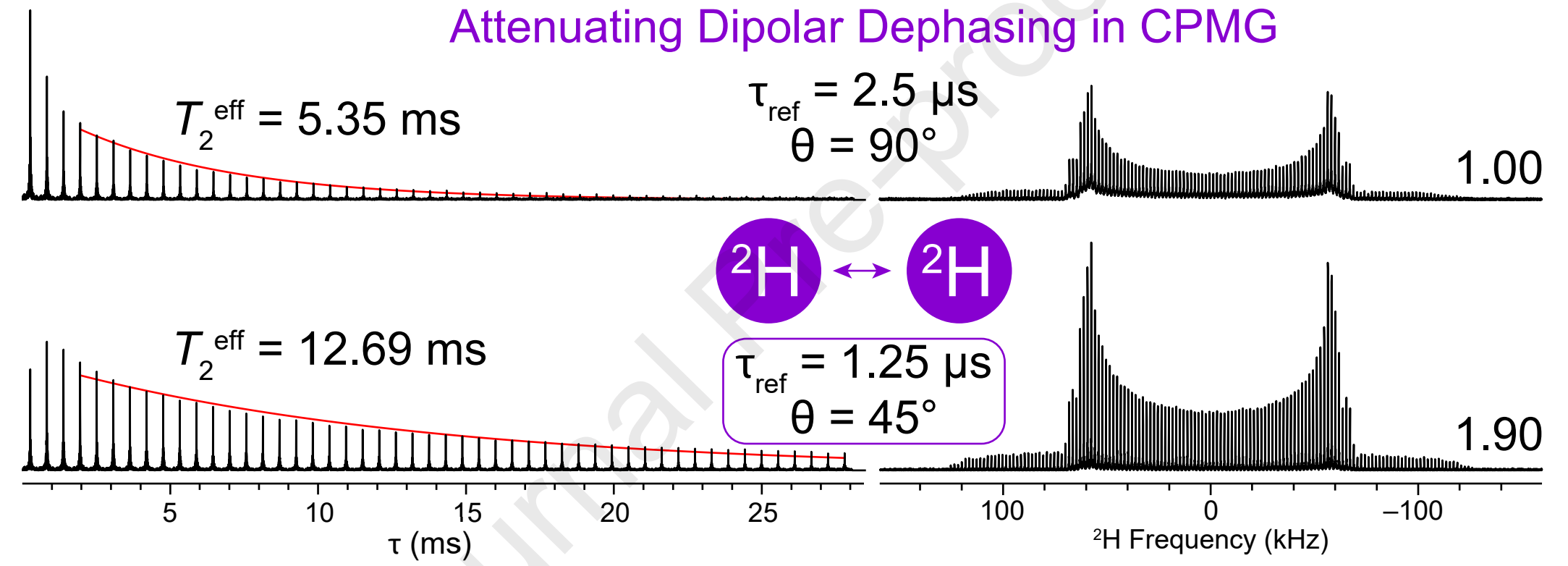
Attenuating Dipolar Dephasing in CPMG
$T_2^{eff}$ = 5.35 ms
$\tau_{ref}$ = 2.5 µs
θ = 90°
1.00
$^2H \leftrightarrow ^2H$
$T_2^{eff}$ = 12.69 ms
$\tau_{ref}$ = 1.25 µs
θ = 45°
1.90
5
10
15
20
25
τ (ms)
100
0
–100
$^2H$ Frequency (kHz)

**Declaration of interests**

☒ The authors declare that they have no known competing financial interests or personal relationships that could have appeared to influence the work reported in this paper.

☐ The authors declare the following financial interests/personal relationships which may be considered as potential competing interests:

Journal Pre-proofs